BAUHAUS UNIVERSITY
GRADUATE SCHOOL OF STRUCTURAL ENGINEERING

Extension of the Uniform Material Law for High Strength Steels

Master's Thesis by Sinan Korkmaz

Supervised by Prof. Joachim W. Bergmann

2008

Submitted as a partial requirement of Advanced Mechanics of Materials and Structures course at Graduate School of Structural Engineering, Bauhaus University

Table of Contents

Acknowledgments

First and foremost I wish to express my sincere thanks and appreciation to Prof. Joachim W. Bergmann for his time, patience, understanding, attention, guidance, insight, and support during the preparation of this thesis.

In addition, special thanks are due to my girlfriend, Tugba Karagoz, and to my family for their supports although they are thousands of kilometers far away from me.

Nomenclature

ε_{max}	Maximum Strain
ε_{min}	Minimum Strain
$\Delta\varepsilon$	Strain Range
ε_a	Strain Amplitude
$\varepsilon_{a,el}$	Elastic Strain Amplitude
$\varepsilon_{a,pl}$	Plastic Strain Amplitude
σ_a	Stress Amplitude
E	Young ’s Modulus
K’	Cyclic Strength Coefficient
n’	Cyclic Strain Hardening Exponent
ε_m	Mean Strain
σ_m	Mean Stress
σ_{max}	Maximum Stress
σ_{min}	Minimum Stress
$\Delta\sigma$	Stress Range
R	Stress Ratio ($\frac{\sigma_{min}}{\sigma_{max}}$)
t	Time
σ_f’	Fatigue Strength Coefficient
b	Fatigue Strength Exponent
ε_f’	Fatigue Ductility Coefficient
c	Fatigue Ductility Exponent
R_m	Ultimate Tensile Strength
N	Number of Load Cycles to Crack Initiation
σ_E	Endurance Stress

$\mathbf{N_E}$	Number of Cycles at Endurance Limit
$\mathbf{P_{SWT}}$	Smith,Watson and Topper Damage Parameter
$\boldsymbol{\rho}$	Notch Radius
$\mathbf{K_t}$	Stress Concentration Factor
$\mathbf{S_{a,E}}$	Nominal Stress Amplitude at Endurance
$\mathbf{m}$	Weibull Exponent
$\mathbf{A_{eff}}$	Effective Area
$\mathbf{V_{eff}}$	Effective Volume
$\boldsymbol{\chi^*}$	Normalized Stress Gradient
$\mathbf{n_\sigma}$	Support Factor for Stress Gradient
$\mathbf{f_r}$	Roughness Factor
$\mathbf{f_{st}}$	Statistical Size Factor
$\mathbf{S_{aE,area}}$	Nominal Stress Amplitude Calculated via Area
$\mathbf{V}$	Volume
$\mathbf{S_{aE,vol}}$	Nominal Stress Amplitude Calculated via Volume
$\mathbf{S_{aE,min}}$	Minimum Nominal Stress Amplitude
$\mathbf{S_{aE,exp}}$	Nominal Stress Amplitude Obtained from Experiments
$\mathbf{A_{standard}}$	Standard Area
$\mathbf{V_{standard}}$	Standard Volume
$\boldsymbol{\sigma_{aE}}$	Stress Amplitude at Endurance
$\mathbf{R_z}$	Average Roughness of Surface

List of Tables

List of Figures

1. Introduction

1.1. History of Fatigue

Fatigue concept includes a large number of phenomena of delayed damage and fracture under loads and environmental conditions. Most of component designs include elements exposed to cyclic loads. Such loading leads to cyclic stresses that habitually result in failure owing to fatigue. About 95% of all structural failures occur through a fatigue mechanism. [1]

The damage resulting from fatigue process is cumulative and unrecoverable, because:

It is hardly possible to notice any deterioration in behavior of the material throughout the fatigue procedure. Hence, failure comes into being without warning.

Any improvement in the fatigue behavior of the material is not possible even if the material is kept at rest for a period of time.

In the early times, it was known that timber and metals are prone to be broken by bending them repeatedly with large amplitudes. Eventually, it is discovered that fatigue failures can come into being even with stress amplitudes within elastic range of the material. In the nineteenth century, the failures in the railroad coach axles have become a common problem especially in the developed countries of this era. This situation has made the engineers focus on fatigue problems. Between 1852 and 1870, the railroad engineer August Wöhler conducted the first systematic fatigue investigation. Wöhler introduced the concept of the fatigue curve, the diagram where a characteristic magnitude of cyclic stress is plotted against the cycle number until fatigue failure. The following diagram, which shows the relationship between the nominal stress and the number of cycles to failure, is prepared by Wöhler for Krupp steel company:

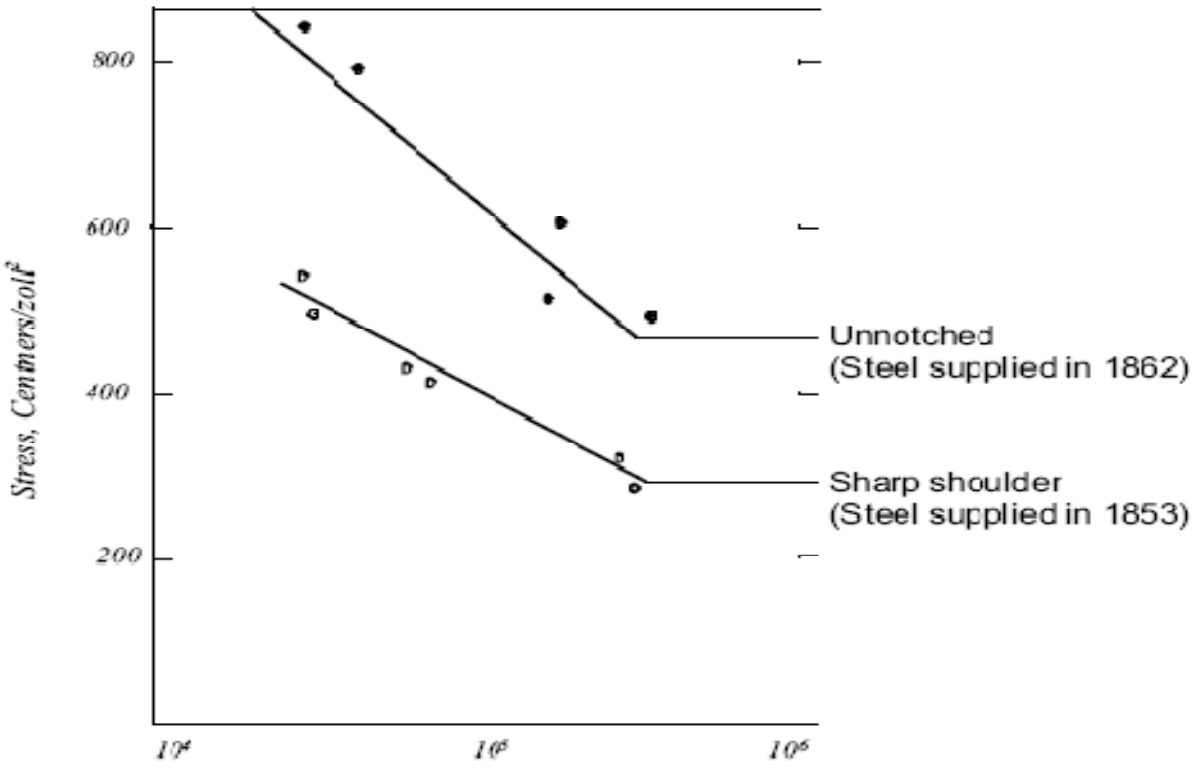

Figure 1. Wöhler's S–N Curve for Krupp Axle Steel

Then, in the first part of the twentieth century, the engineers strived to find out the mechanisms of the fatigue process. Investigations carried out on bridges, marine structures and power generation machines let Manson and Coffin find out a local strain methodology to explain crack initiation with linear elastic fracture mechanics. This methodology has let the engineers design fatigue resistant components without merely relying on experimental results.

1.2. Physics of Fatigue

The physical growth of a crack is normally divided into 2 detach stages. These stages are the crack initiation phase and the crack growth phase. Cracks resulting from fatigue initiate through shear strain energy release. The shear stresses bring about local plastic deformation along the slip planes. During the sinusoidal cycles, the slip planes move back and forth. This movement results in small extrusions and intrusions on the crystal surface. Consequently, embryonic cracks are created by the surface disturbances, which are 1 to 10 microns in height.

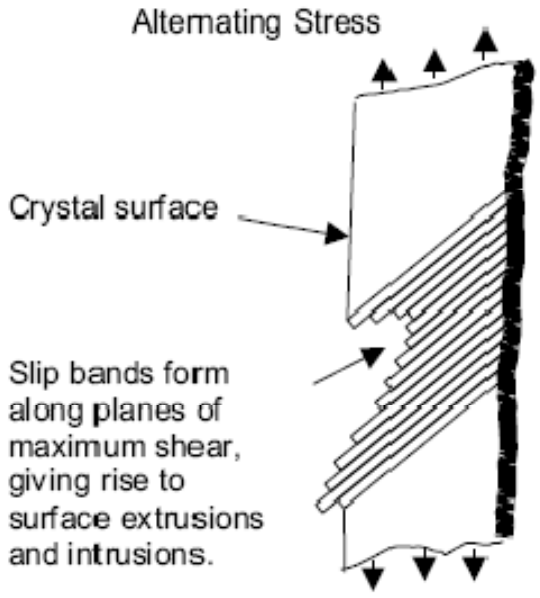

Figure 2. Surface Extrusions and Intrusions

Fatigue is considered to be a gradual process of the accumulation of damage. It advances on different levels beginning from the scale of the crystal lattice, dislocations and other objects of solid state physics up to the scales of structural components. Four stages of fatigue damage are usually distinguishable in this sense. The first stage is at microstructure level. Grains and intergranular layers are of concern at the instance of polycrystalline alloy. The damage is diffused over the most stressed parts of the structural component. Nuclei of macroscopic cracks originate, and grow under the eventual loading at the end of this stage. Surface nuclei usually can be monitored with proper magnification. At the second stage the growth of cracks of which depth is small compared with the size of the cross section occurs. The sizes of these cracks are equal to a few characteristic scales of microstructure, i.e., grains. These cracks are so-called short cracks. Their propagation way is different from that of wholly developed macroscopic cracks. These cracks find their way through the nonhomogeneous material. Most of them discontinue growing upon confronting some hindrance, however, one or several cracks transform into macroscopic, so-called long fatigue cracks that propagate in a direct way as strong stress concentrators. This procedure shapes the third stage of fatigue damage. The fourth stage is considered to be the swift final structure due to the sharp stress focus at the crack front. [2]

Damage mode and fracture are affected by environmental conditions. The plasticity of most materials increases at high temperatures. Moreover, metals creep, and polymers show

thermo-plastic behavior. On the other hand, at lower temperatures, metals show less plasticity and become more brittle. If a component is exposed to a multi-affect of uneven thermal conditions and cyclic loading, some fixed phenomena come into being, such as creep fatigue, creep accelerated by vibration, and thermo-fatigue. In highly corrosive situations, corrosion fatigue, the combination of fatigue and corrosion, comes into being. What is more, hydrogen and irradiation embrittlement, various wear ageing processes, interact with fatigue. Delayed fracture can occur under even constant or slowly changing loading. Crack initiation and propagation in metals under the combination of active environment and non-cyclic loads is a typical instance for such situations. This type of damage is called corrosion cracking. These phenomena are under the concept of "static fatigue".

Once the crack reaches to the grain boundary, the mechanism is progressively transmitted to the neighboring grain. After growing through about 3 grains, the crack changes its propagation direction. At the first stage, the growth direction is the maximum shear plane, being 45° to the direction of loading. On the other hand, at the second stage, since the crack is large enough to form a geometrical stress concentration, a tensile plastic zone is shaped at the tip of the crack. Then, the crack grows perpendicular to the load direction.

Fatigue initiation is induced by local plastic strains, which is not the case in Wöhler's S-N analysis. Merely elastic stresses are used in the method developed by Wöhler, which is commonly known S-N fatigue analysis. Furthermore, S-N analysis does not differentiate the foregoing two phases of crack growth. Thus, another approach is needed in order to make predictions in terms of fatigue.

1.3. Strain Based Approach

Sandglass-shaped specimens are used in fatigue tests. The specimens are subjected to different types of cyclic loading, such as: small-scale bending, torsion, tension, and compression. The results of these tests are plotted in terms of strain versus cycles to failure on an E-N diagram. In this work, strain-based approach is used for the reason that it does not involve the above mentioned disadvantages of S-N approach.

1.4 Strain Cycles

There are three different types of cyclic strains that contribute to the fatigue process.

The following figure illustrates a fully-reversed strain cycle with a sinusoidal form.

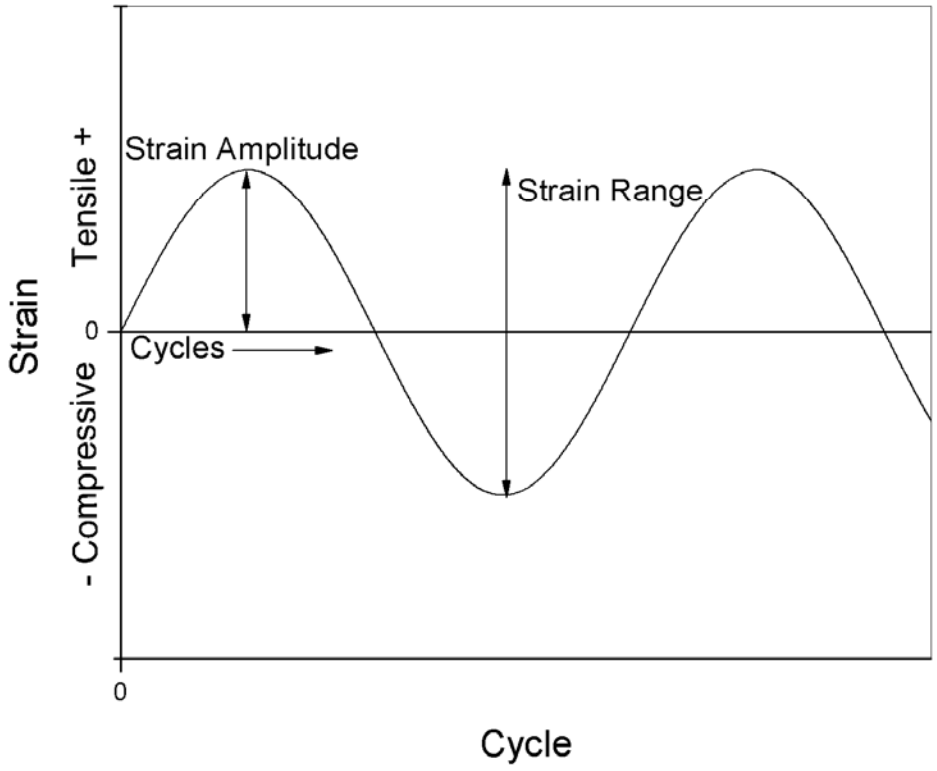

Figure 3. Fully-Reversed Strain Cycle with Sinusoidal Form

This idealized loading condition is typical in rotating shafts operating at constant speed without overloads. This type of strain cycle is used for most of the fatigue tests.

The maximum strain (ε_{max}) and minimum strain (ε_{min}) are of equal magnitude but opposite sign. Conventionally, tensile strain is considered to be positive and compressive strain negative. The strain range, $\Delta\varepsilon$, is equal to the algebraic difference between the maximum and minimum strains in a cycle.

$$\Delta\varepsilon = \varepsilon_{max} - \varepsilon_{min}$$

The strain amplitude, ε_a, equals to one half the strain range.

$$\varepsilon_a = \Delta\varepsilon / 2 = (\varepsilon_{max} - \varepsilon_{min}) / 2$$

There are two component parts of strain amplitude: Elastic strain amplitude and plastic strain amplitude:

$$\varepsilon_a = \varepsilon_{a,el} + \varepsilon_{a,pl}$$

Where

$$\varepsilon_{a,el} = \sigma_a / E$$

and

$$\varepsilon_{a,pl} = (\sigma_a / K')^{1/n'}$$

That is,

$$\varepsilon_a = \sigma_a / E + (\sigma_a / K')^{1/n'}$$

The following figure illustrates the more general situation where the maximum strain and minimum strain are not equal:

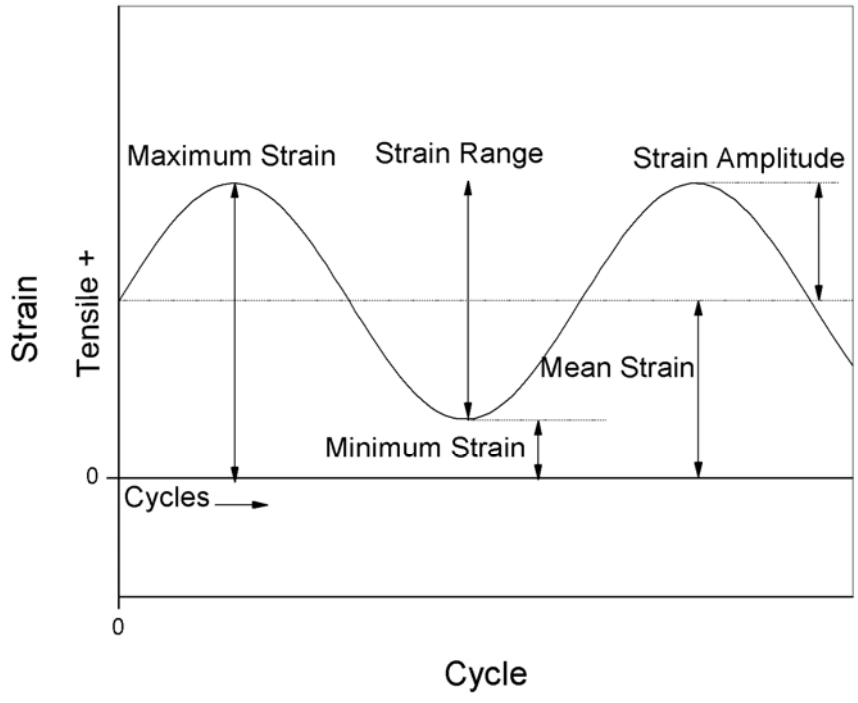

Figure 4. Common Strain Cycle Graph

In this case, the strains are both tensile and characterize a mean offset:

$$\varepsilon_m = (\varepsilon_{max} + \varepsilon_{min}) / 2$$

Cyclic strain-time graph and the corresponding hysteresis loops can be obtained via Incremental Step Test.

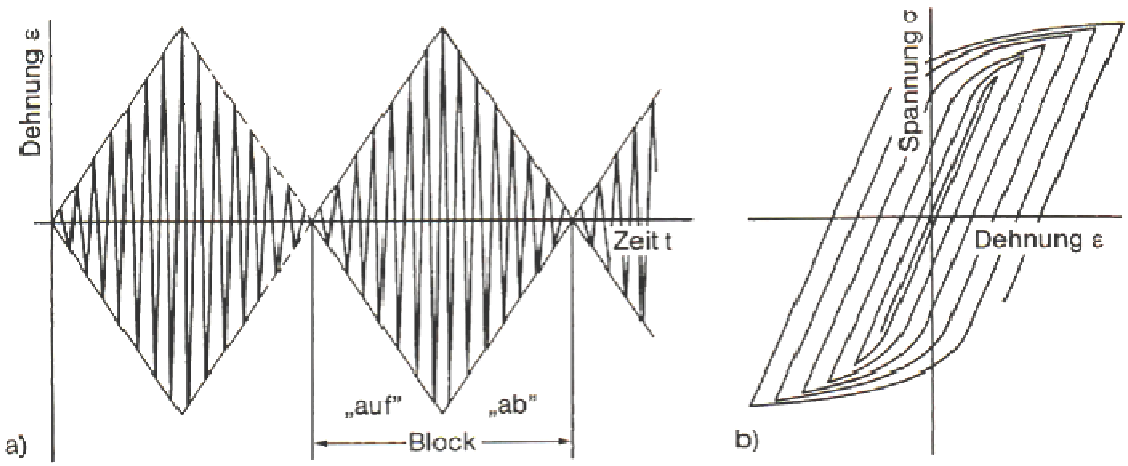

Figure 5a. Strain – Time Graph
Figure 5b. Hysteresis Loops

Cyclic hardening or softening of the material is reflected by a reduction or an increase, respectively, in the axial strain amplitude. Similarly, under constant amplitude, strain-controlled fatigue loading, cyclic hardening or softening of the material cause an increase or decrease, respectively in the axial stress amplitude. [3]

The strain-stress graph of a cyclic loading is schematically as follows:

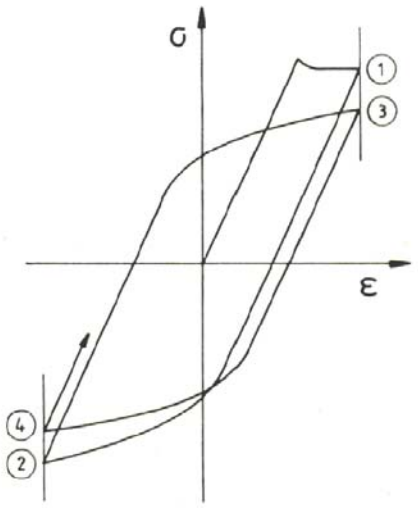

Figure 6. Softening Behavior at Strain-Controlled Test

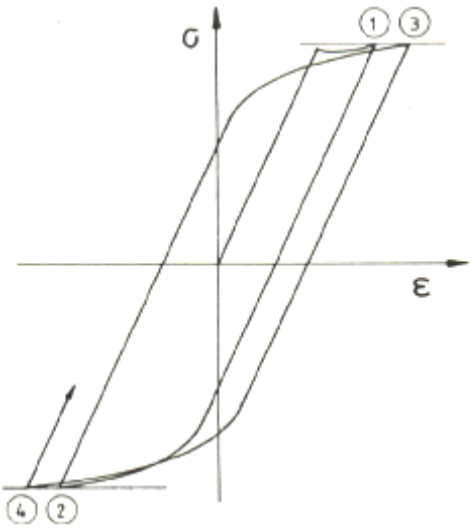

Figure 7. Softening Behavior at Stress-Controlled Test

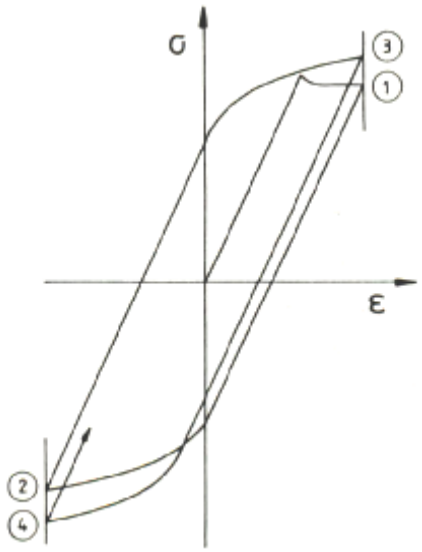

Figure 8. Hardening Behavior at Stress-Controlled Test

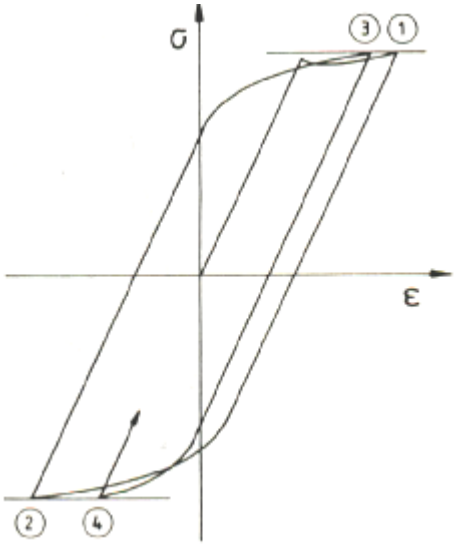

Figure 9. Hardening Behavior at Strain-Controlled Test

of which strain-time and stress-time conditions are below:

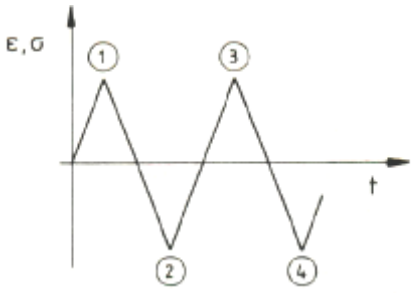

Figure 10. Strain – Time and Stress – Time Conditions

Fatigue is generally divided into two parts in terms of number of load cycles: High-cycle and low-cycle fatigue. The behavior is considered in high-cycle fatigue if plastic deformations are small enough and localized in the vicinity of the crack tip and the main part of the body is deformed elastically. On the other hand, the behavior is considered within low-cycle fatigue area if the cyclic loading accompanied by elasto-plastic deformations in the bulk of the body. Practically, one can consider it as low-cycle fatigue if the cycle number up to the initiation of an observable crack or until final fracture is below 10^4 or $5 \cdot 10^4$ cycles.

Every cycle encloses maximum magnitudes and minimum magnitudes of the applied stresses. A cycle is characterized as a segment of the loading process limited with two adjacent up-crossings of the mean stress:

$$\sigma_m = (\sigma_{max} + \sigma_{min}) / 2$$

The cyclic loading is typically explained by the stress amplitude:

$$\sigma_a = (\sigma_{max} - \sigma_{min}) / 2$$

or the stress range:

$$\Delta\sigma = \sigma_{max} - \sigma_{min}$$

Stress ratio is an additional major characteristic of the cyclic loading:

$$R = \sigma_{min} / \sigma_{max}$$

For symmetrical cycles, $R = -1$.

If a cycle encloses merely non-negative stresses, $R > 0$.

Despite the fact that the cycle number N is an integer number, it is treated as a continuous variable in the calculations in this thesis for the sake of computation simplicity.

Some types of cyclic loading are shown schematically in the following figure:

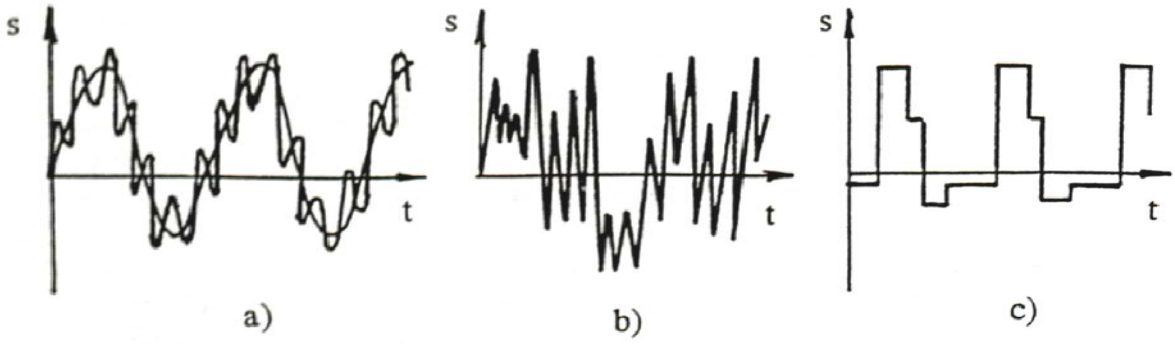

Figure 11. Cyclic Loading Processes

Figure 11a. Biharmonic Process

Figure 11b. Pseudo-Stochastic Process

Figure 11c. Piecewise Process

There are biharmonic, pseudo-stochastic, and piecewise constant processes among these types. Stochastic processes are often met in practice. These processes vary as narrow-band or broadband, stationary or nonstationary.

A generalization of cycle loading is block loading. One block means one of the repeated stages during the service of a structure. A block of loading corresponding to one standard flight of an aircraft can be mentioned as an example. Such a block contains loads during ground motions, take-off and landing, climb, cruise, and descent flights. Every block comprises of a large number of cycles. If the number of blocks in the service life of a structure is adequately large, each block can be treated as a compound cycle. [2] A schematic representation of a compound cycle is as follows:

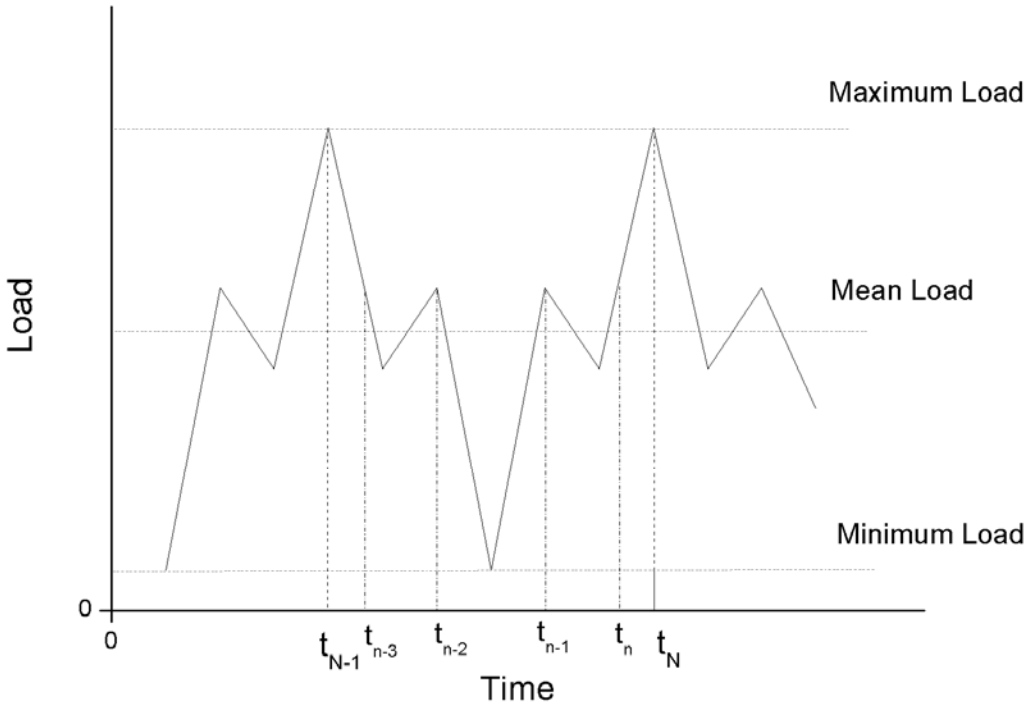

Figure 12. Compound Cycle Containing Interior Cycles

The compound cycle comprises of the loading between $t_{N-1} - t_N$ time interval. Within this compound cycle, there are two interior cycles, namely, the loading between $t_{n-3} - t_{n-2}$ and $t_{N-1} - t_N$ time intervals.

2. Uniform Material Law (UML)

The uniform material law was proposed by Bäumel and Seeger in 1990. It has been derived from a large amount of fatigue data collected by them. This method is akin to universal slopes method, which assigns different slopes to unalloyed and low-alloy steels and to aluminum and titanium alloys respectively.[10] UML is a handy and user-friendly method since only the tensile strength of the material is needed for estimation of the strain-life curve, in contrast to other methods, such as four-point correlation method, universal slopes method, Mitchell's method, modified universal slopes method, which also require the data of the reduction in area or the fracture ductility of the material. Using the fatigue data collected, the prediction capability of the uniform material law and the modified universal slopes method are checked by Bäumel and Seeger. They realized that both methods demonstrate larger

deviations between the predicted and experimental results for aluminum and titanium alloys and for high-alloy steels, compared with unalloyed and low-alloy steels. They put forward different estimates for low-alloy steels and for aluminum and titanium alloys. The following table depicts the values, on which UML is based:

	for unalloyed and low-alloyed steel	for aluminum and titanium-alloy
σ_f'	$1,5 \cdot R_m$	$1,67 \cdot R_m$
b	-0,087	-0,095
ε_f'	$0,59 \cdot \psi$	0,35
c	-0,58	-0,69
σ_D	$0,45 \cdot R_m$	$0,42 \cdot R_m$
ε_D	$0,45 \cdot \left(\frac{R_m}{E}\right) + 1,95 \cdot 10^{-4} \cdot \psi$	$0,42 \cdot \frac{R_m}{E}$
N_D	$5 \cdot 10^5$	$1 \cdot 10^6$
K′	$1,65 \cdot R_m$	$1,61 \cdot R_m$
n′	0,15	0,11
	$\psi = 1,0 \quad \text{for}: \frac{R_m}{E} \leq 3 \cdot 10^{-3}$ $\psi = \left(1,375 - 125,0 \cdot \frac{R_m}{E}\right) \quad \text{for}: \frac{R_m}{E} > 3 \cdot 10^{-3}$ and $\psi \geq 0$	

Table 1. Uniform Material Law

3. Strain-Load Cycle Computation

Basquin linearized the stress-life data via:

$$\sigma_a = \sigma_f' \cdot (2N)^b$$

Then, Manson and Coffin carried out linearization plastic strain-life data by using power law function:

$$\varepsilon_{a,pl} = \varepsilon_f' \cdot (2N)^c$$

If we introduce these equations into the total strain equation:

$$\varepsilon_a = \varepsilon_{a,el} + \varepsilon_{a,pl}$$

$$\varepsilon_{a,el} = \sigma_f' / E \cdot (2N)^b$$

$$\varepsilon_a = \sigma_f' / E \cdot (2N)^b + \varepsilon_f' \cdot (2N)^c$$

The obtained equation is the basis of strain-life computations in this study.

$$\psi = 1{,}375 - 125 (R_m / E)$$

for

$$R_m / E \leq 3 \cdot 10^{-3}$$

and

$$\psi = 1$$

for

$$R_m / E > 3 \cdot 10^{-3}$$

$$\varepsilon_f' = 0.59 \psi$$

$$\sigma_f' = 1.5 R_m$$

The values are used in accordance with the Table 1 for the first approach, which shall be called as “Conventional UML” hereafter. On the other hand, in the second approach, a new set of values are presented. The second approach shall be called as “Extended UML” throughout this thesis (see Table 2 and Table 3).

4. Outcomes of Uniform Material Law

4.1. Stress Amplitude-Strain Amplitude Outcomes of Conventional Uniform Material Law

The following graph represents the stress amplitude – strain amplitude relationship in accordance with the conventional UML in a linear way for steels that are used in this study:

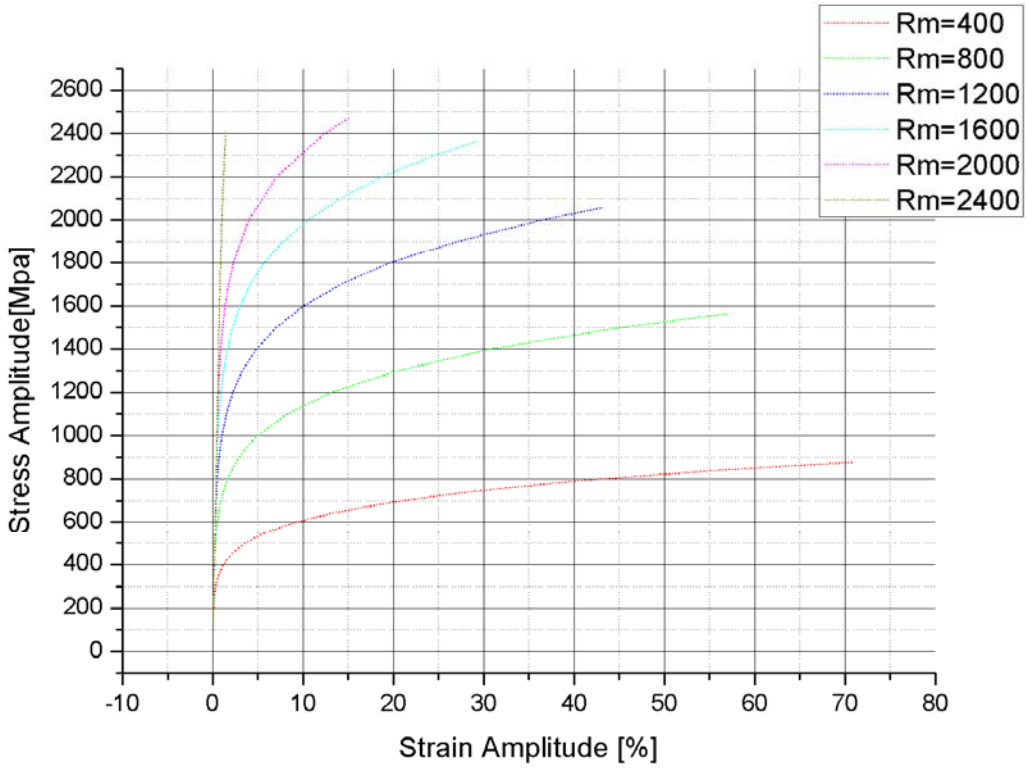

Figure 13. Stress Amplitude – Strain Amplitude Relationship Calculated with the Conventional UML in Linear Scales

The same data can be depicted via such a logarithmic graph:

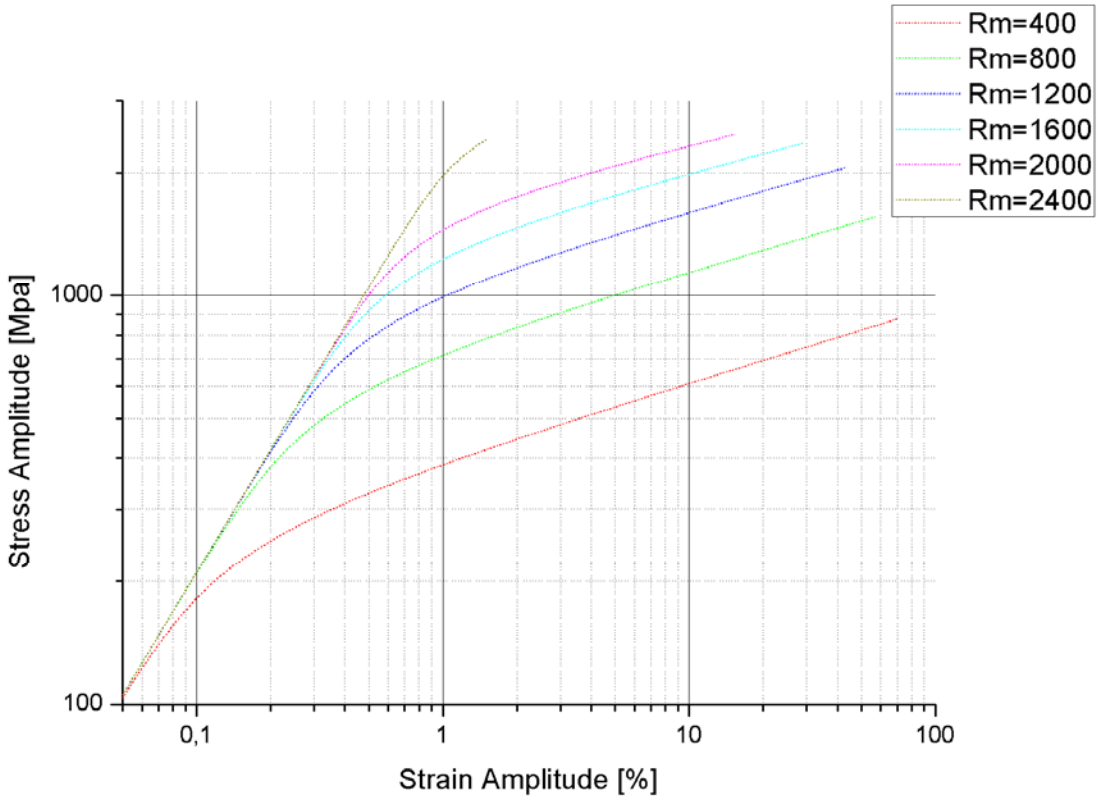

Figure 14. Stress Amplitude – Strain Amplitude Relationship Calculated with the Conventional UML in Logarithmic Scales

The above data is processed via the given equations and conventional UML. The results are represented in the following part.

4.2 Strain Amplitude – Load Cycle Behavior Outcomes of Conventional Uniform Material Law

The strain amplitude - load cycle behavior of the steel with the tensile strength of 400 MPa is calculated and represented by the following graph:

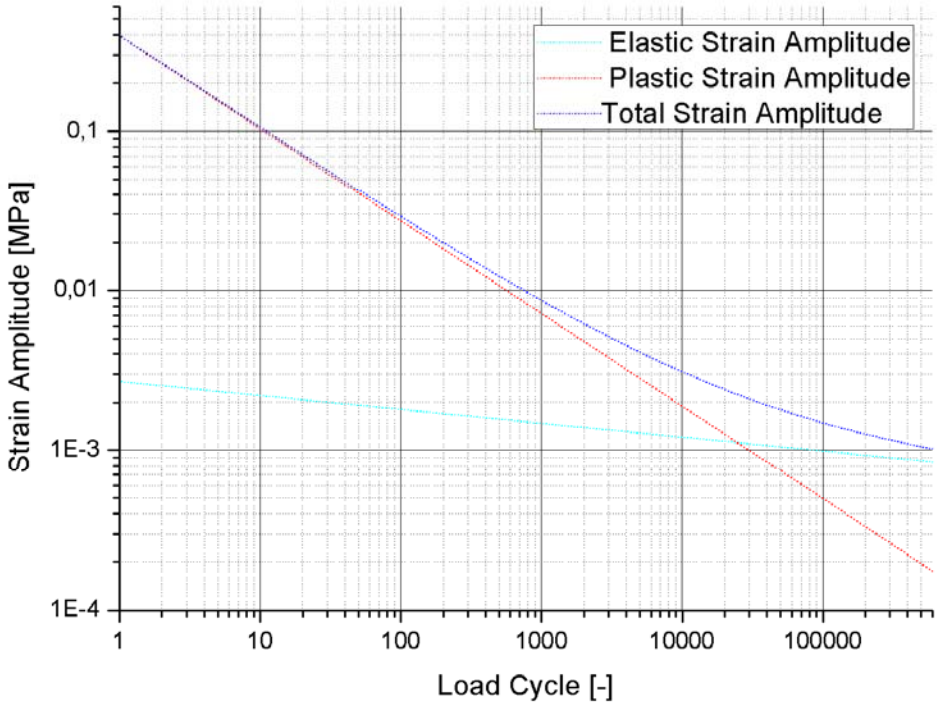

Figure 15. Strain Amplitude – Load Cycle Graph for the Steel with the Tensile Strength of 400 MPa in Accordance with the Conventional UML

The total strain amplitude at 500000th cycle is calculated as 0,001054 for R_m= 400

The plastic strain amplitude is greater than the elastic strain amplitude for a large amount of load cycles.

At the strain amplitude - load cycle behavior of the steel with the tensile strength of 800 MPa, the plastic strain amplitude is significantly lower compared to the steel with the tensile strength of 400 MPa:

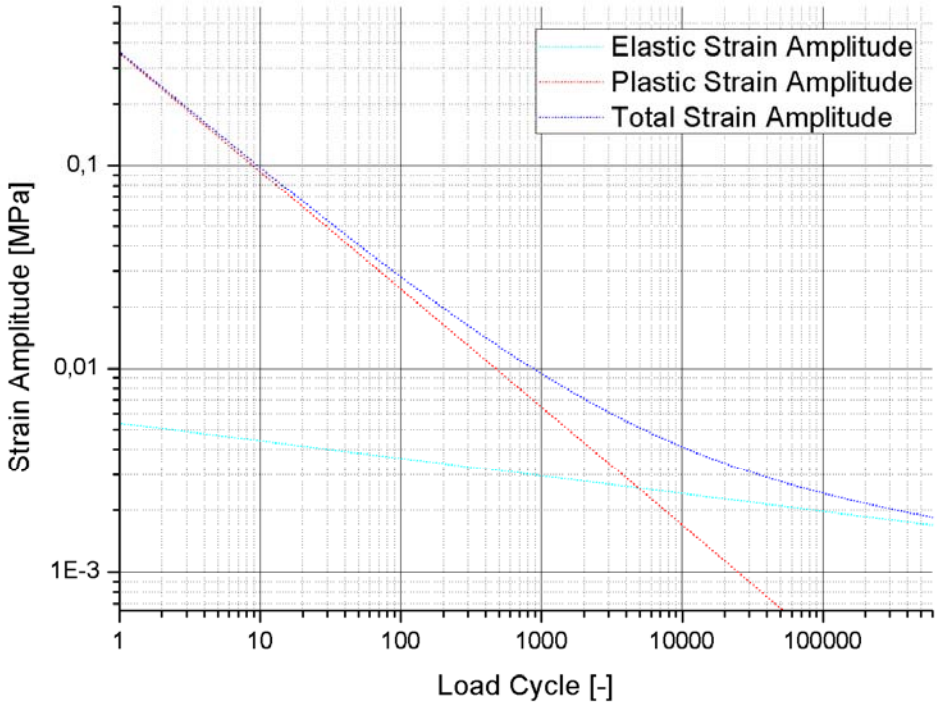

Figure 16. Strain Amplitude – Load Cycle Graph for the Steel with the Tensile Strength of 800 MPa in Accordance with the Conventional UML

The total strain amplitude at 500000th cycle is 0,001893 for $R_m = 800$

In the case of $R_m = 1200$, the plastic strain amplitude is higher than the elastic strain amplitude just for the first 1000 load cycles:

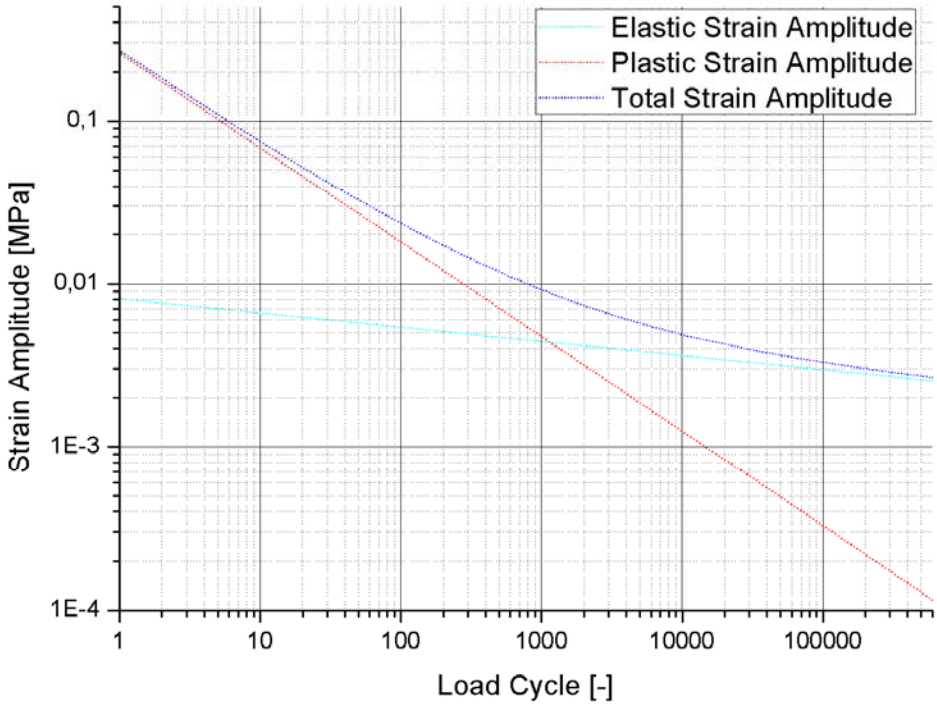

Figure 17. Strain Amplitude – Load Cycle Graph for the Steel with the Tensile Strength of 1200 MPa in Accordance with the Conventional UML

The total strain amplitude at 500000th cycle equals to 0,002706 for $R_m = 1200$

For $R_m = 1600$, the elastic strain amplitude is larger than the plastic strain amplitude all throughout the service life:

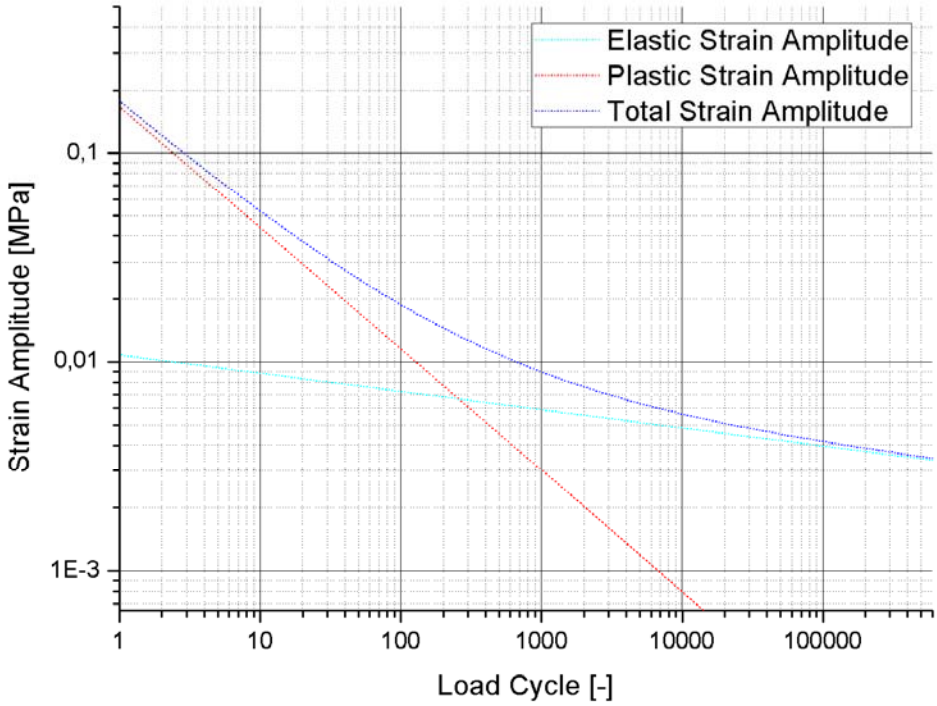

Figure 18. Strain Amplitude – Load Cycle Graph for the Steel with the Tensile Strength of 1600 MPa in Accordance with the Conventional UML

The total strain amplitude at 500000th cycle becomes 0,003518 for $R_m = 1600$

For $R_m = 2000$, the plastic strain amplitude so small that the elastic strain amplitude and the total strain amplitude become close to each other:

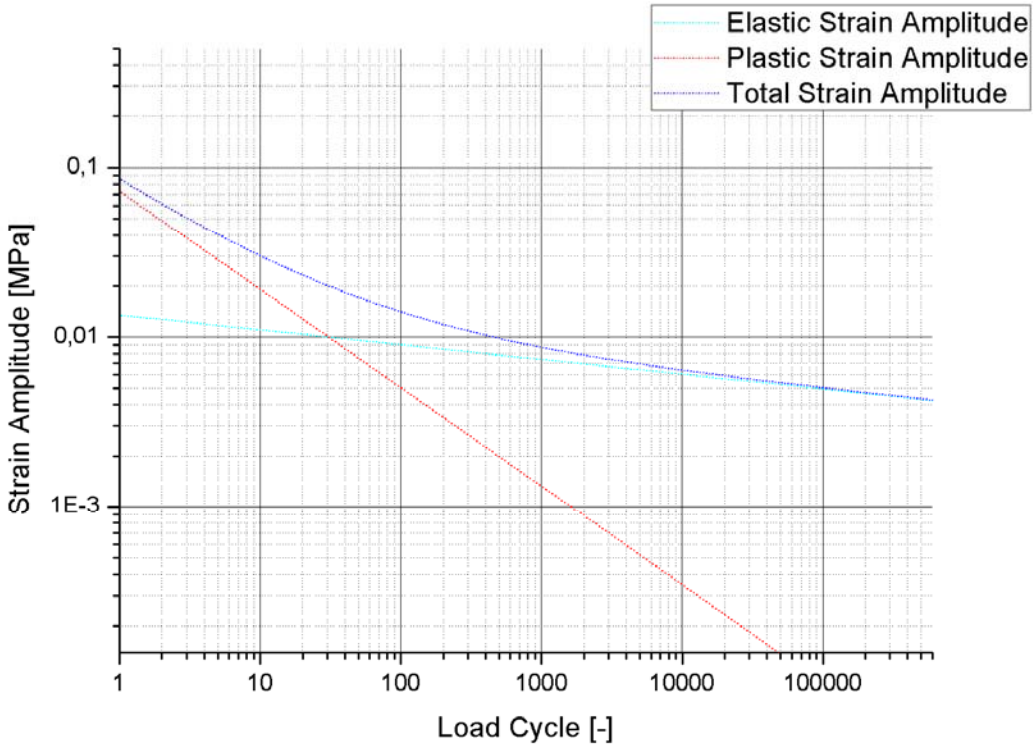

Figure 19. Strain Amplitude – Load Cycle Graph for the Steel with the Tensile Strength of 2000 MPa in Accordance with the Conventional UML

The total strain amplitude at 500000th cycle is equal to 0,00433 for $R_m = 2000$

Finally, the elastic strain amplitude and the total strain amplitude become the same as the plastic strain amplitude is zero for the steel with the tensile strength of 2400 MPa:

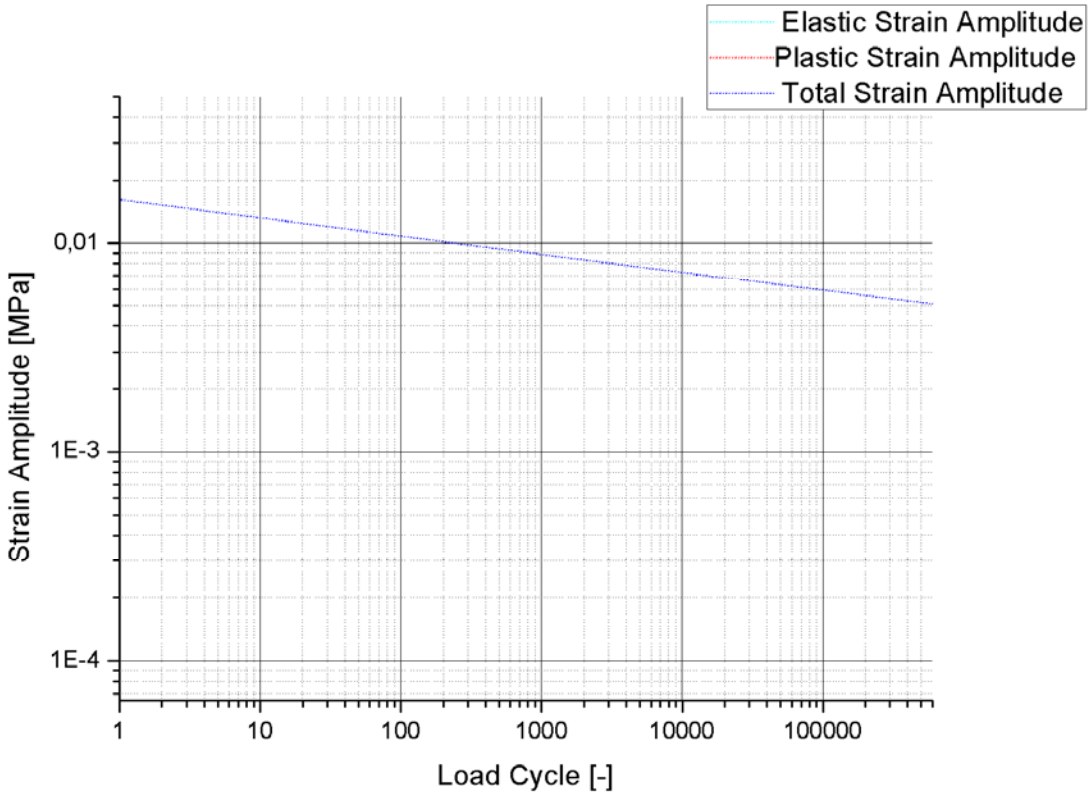

Figure 20. Strain Amplitude – Load Cycle Graph for the Steel with the Tensile Strength of 2400 MPa in Accordance with the Conventional UML

The total strain amplitude at 500000th cycle is calculated as 0,005153 for $R_m = 2400$

5. Extension of UML

Then, a new calculation is carried out with an extension of UML. The extension is as follows:

In the first approach, ψ is applied to ε_f' only:

$$\varepsilon_f^{'} = 0.59\ \psi$$

In this calculation, the elastic strain amplitude is:

$$\varepsilon_{a,el} = \sigma_f^{'} / E\ (2N)^b$$

where

$$b = - \log (\sigma_f' / \sigma_E) / 6$$

$$c = -0.58$$

and

$$\sigma_E = R_m \cdot (0.32 + \psi / 6)$$

On the other hand, in the second calculation, both ε_f' and σ_f' are calculated by using ψ:

$$\sigma_f' = (1 + \psi) \cdot R_m$$

Then, the elastic strain becomes:

$$\varepsilon_{a,el} = (1 + \psi) \cdot R_m / E \cdot (2N)^b$$

ψ is developed that it is

$$1 \text{ at } R_m = 400 \text{ MPa}$$

and

$$0 \text{ at } R_m = 2600 \text{ MPa}$$

5.1. Stress Amplitude-Strain Amplitude Outcomes of Extended Uniform Material Law

Consequently, the stress amplitude – strain amplitude relationship in accordance with the extended UML becomes:

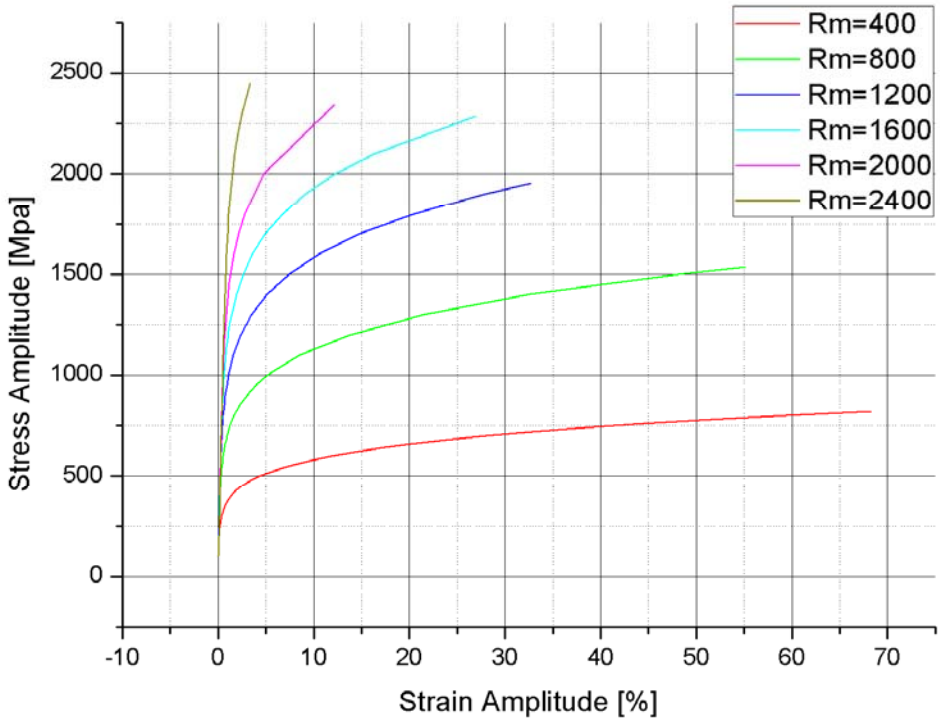

Figure 21. Stress Amplitude – Strain Amplitude Relationship Calculated with the Extended UML in Linear Scales

The estimated strain amplitude – load cycle relations in logarithmic scales are as follows:

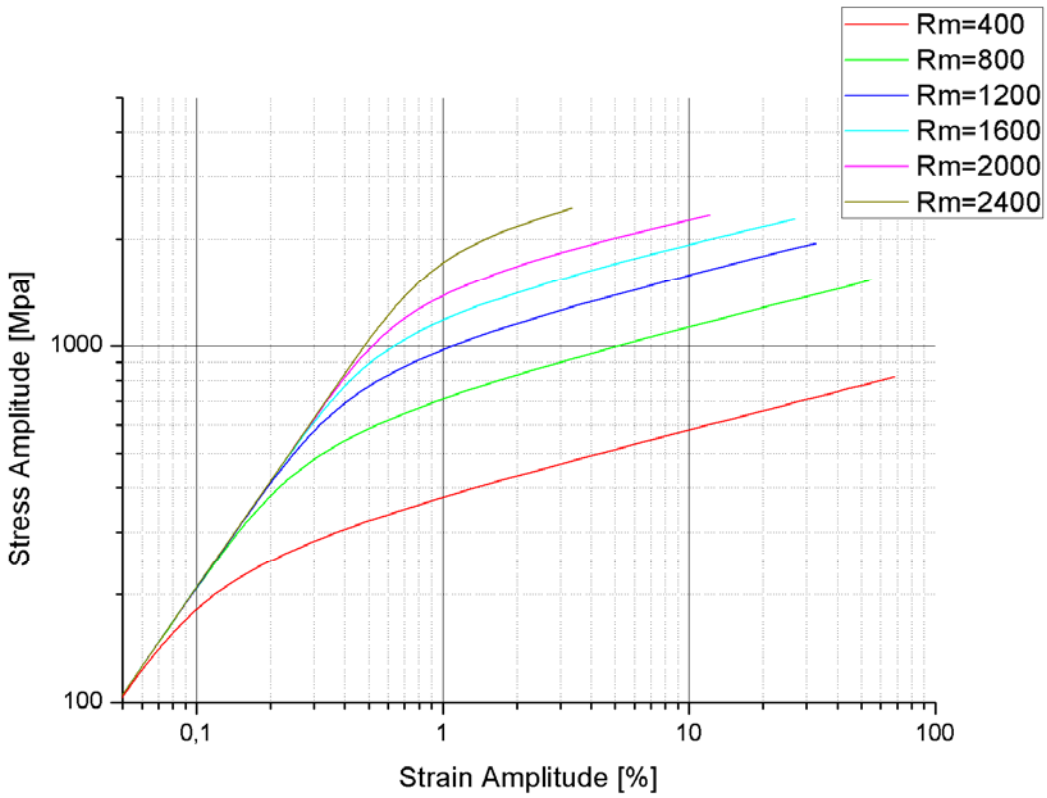

Figure 22. Stress Amplitude – Strain Amplitude Relationship Calculated with the Extended UML in Logarithmic Scales

5.2. Strain Amplitude – Load Cycle Behavior Outcomes of Extended Uniform Material Law

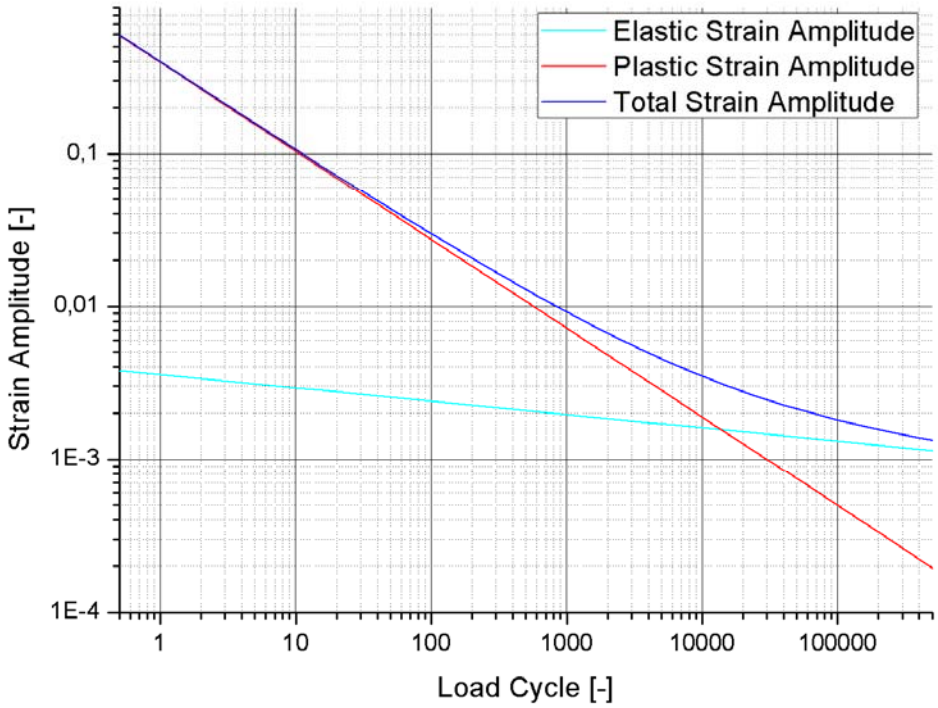

Figure 23. Strain Amplitude – Load Cycle Graph for the Steel with the Tensile Strength of 400 MPa in Accordance with the Extended UML

The elastic strain amplitude is smaller than the plastic strain amplitude until about 15000^{th} load cycle for the steel with $R_m = 400$.

The total strain amplitude at 500000^{th} cycle is calculated as 0.001341 for $R_m = 400$

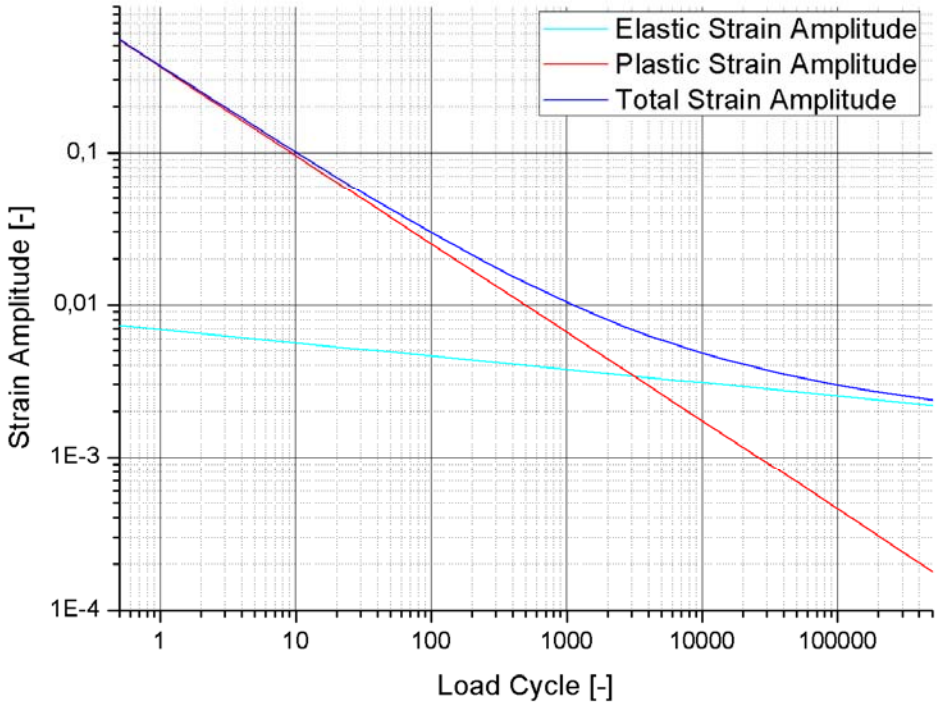

Figure 24. Strain Amplitude – Load Cycle Graph for the Steel with the Tensile Strength of 800 MPa in Accordance with the Extended UML

The intersection point of the elastic strain amplitude and the plastic strain amplitude of the steel with $R_m = 800$ is at an earlier stage than that of the steel with $R_m = 400$. This point is shifted to earlier stages as the tensile strength of the steel gets higher.

The total strain amplitude at 500000^{th} cycle is 0.002379 for $R_m = 800$

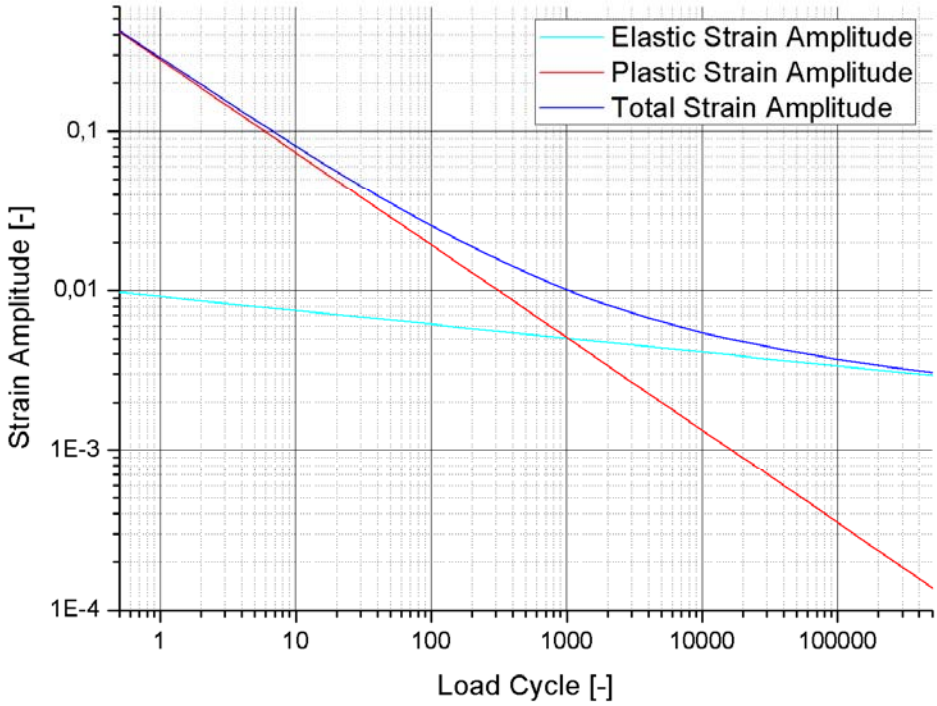

Figure 25. Strain Amplitude – Load Cycle Graph for the Steel with the Tensile Strength of 1200 MPa in Accordance with the Extended UML

The total strain amplitude at 500000^{th} cycle equals to 0.003072 for $R_m = 1200$

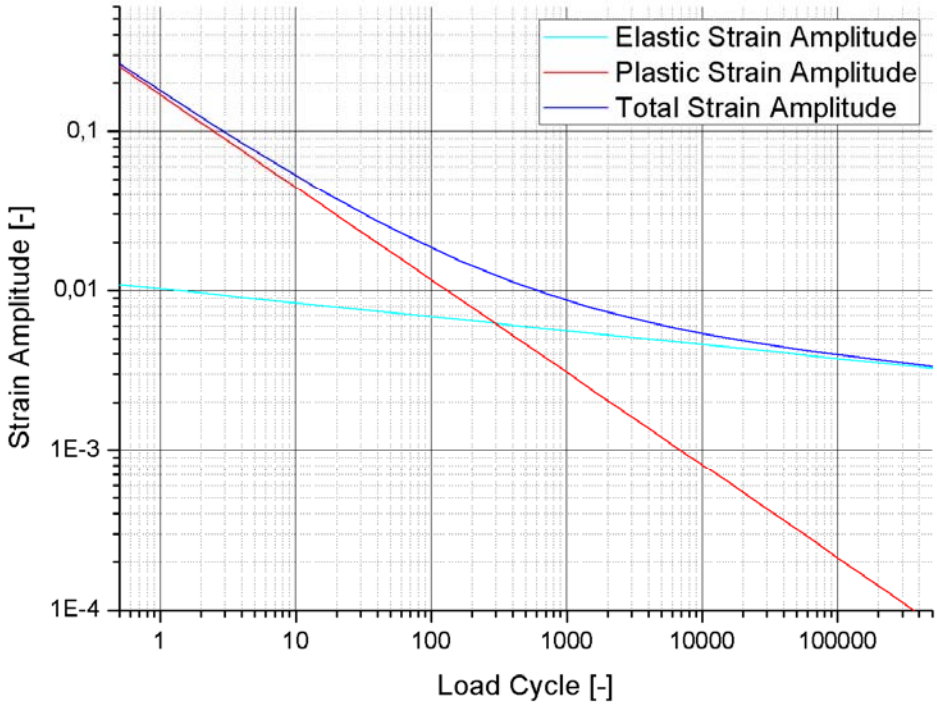

Figure 26. Strain Amplitude – Load Cycle Graph for the Steel with the Tensile Strength of 1600 MPa in Accordance with the Extended UML

The total strain amplitude at 500000^{th} cycle becomes 0.003356 for $R_m = 1600$

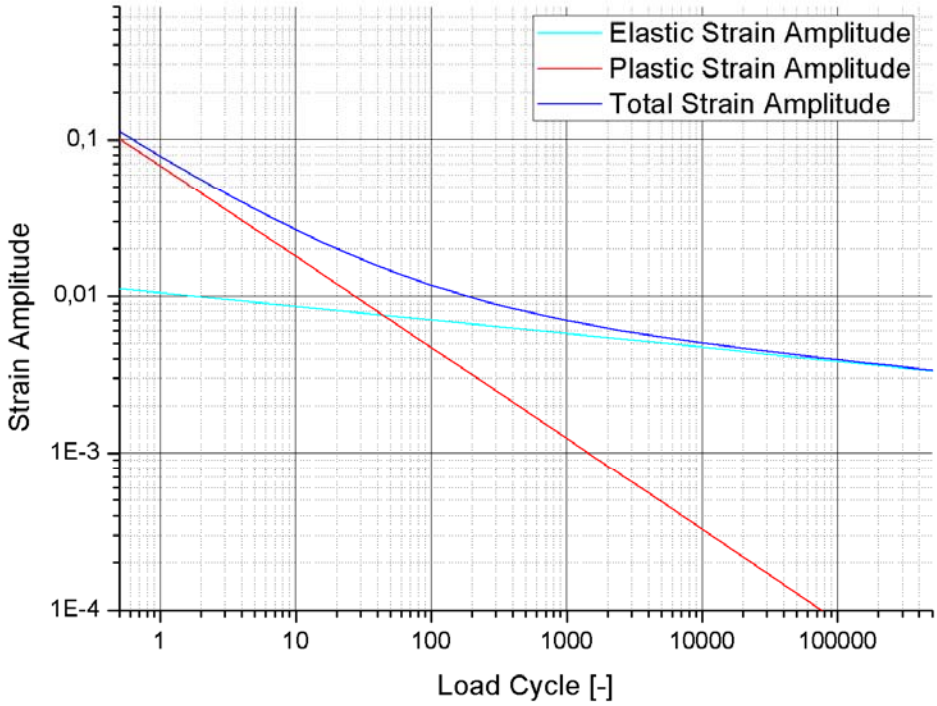

Figure 27. Strain Amplitude – Load Cycle Graph for the Steel with the Tensile Strength of 2000 MPa in Accordance with the Extended UML

The total strain amplitude at 500000th cycle is equal to 0.003391 for $R_m = 2000$

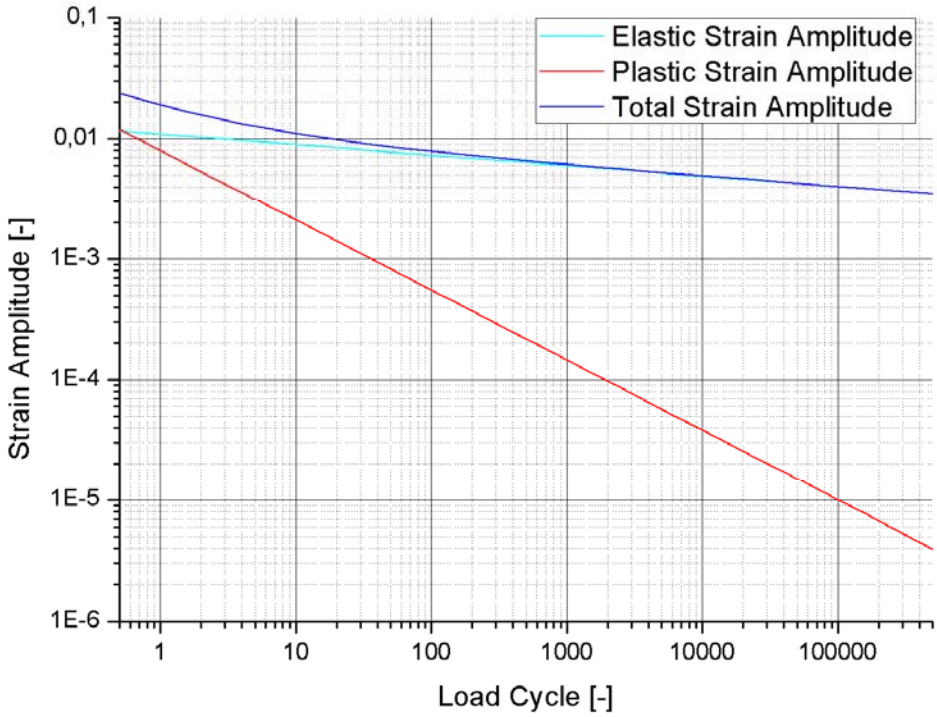

Figure 28. Strain Amplitude – Load Cycle Graph for the Steel with the Tensile Strength of 2400 MPa in Accordance with the Extended UML

The total strain amplitude at 500000th cycle is calculated as 0.003509 for $R_m = 2400$

6. Comparison of Results

6.1. Comparison of the Parameters of Conventional UML and the Extended UML

The calculation results obtained by using UML and extended UML are given in the previous sections. These values are calculated by using the following calculated values:

R_m	400	800	1200	1600	2000	2400
E	210000	210000	210000	210000	210000	210000
K'	660	1320	1980	2640	3300	3960
n'	0.15	0.15	0.15	0.15	0.15	0.15
σ_f'	600	1200	1800	2400	3000	3600
ε_f'	0.590	0.530	0.390	0.249	0.109	0
b	-0.087	-0.087	-0.087	-0.087	-0.087	-0.087
σ_E	180	360	540	720	900	1080
c	-0.58	-0.58	-0.58	-0.58	-0.58	-0.58
N_E	500000	500000	500000	500000	500000	500000
ψ	1	0.898809524	0.66071	0.42262	0.18452	0

Table 2. Values according to the Conventional UML

R_m	400	800	1200	1600	2000	2400
E	210000	210000	210000	210000	210000	210000
K'	878	1709	2374	2844	3275	4240
n'	0.176	0.175	0.170	0.162	0.151	0.143
σ_f'	800	1537	2049	2286	2345	2449
ε_f'	0.590	0.544	0.420	0.259	0.110	0.022
b	-0.1023	-0.10136	-0.0985	-0.0937	-0.0878	-0.0832
σ_E	195	379	526	626	698	776
c	-0.58	-0.58	-0.58	-0.58	-0.58	-0.58
N_E	500000	500000	500000	500000	500000	500000
ψ	1.00000	0.92063	0.70771	0.42884	0.17257	0.02025

Table 3. Values Leading to Final Results of the Extended UML

In the conventional UML,

$$\varepsilon_f' = 0.59 \cdot \psi$$

On the other hand, in the extended UML,

$$\varepsilon_f' = 0.58 \cdot \psi + 0.01$$

$$\psi = 0.5 \cdot (\cos (3.1416 \cdot (R_m - 400) / 2200) + 1)$$

$$\sigma_f' = R_m \cdot (1 + \psi)$$

$$K' = \sigma_f' / (\varepsilon_f')^{n'}$$

$$n' = b / c$$

$$\sigma_E = R_m \cdot (0.32 + \psi / 6)$$

The comparison of the decisive parameters used in the conventional UML and the extended UML are shown in the following graphs and tables:

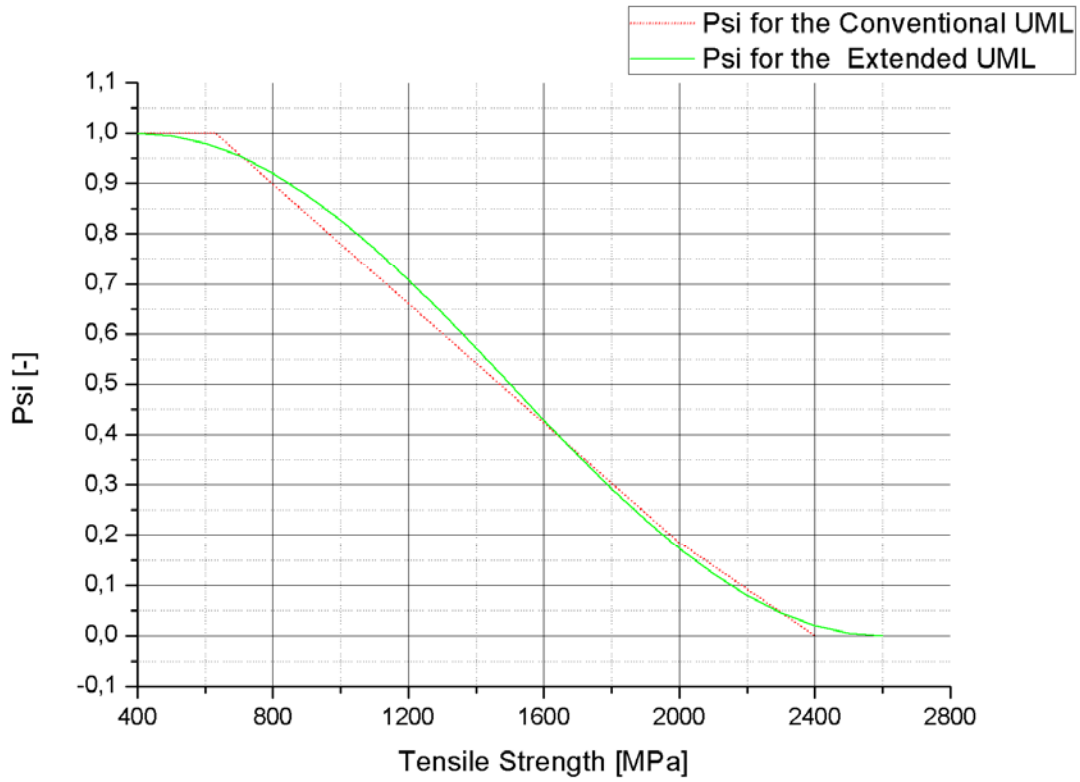

Figure 29. Used ψ Values with Respect to Tensile Strengths

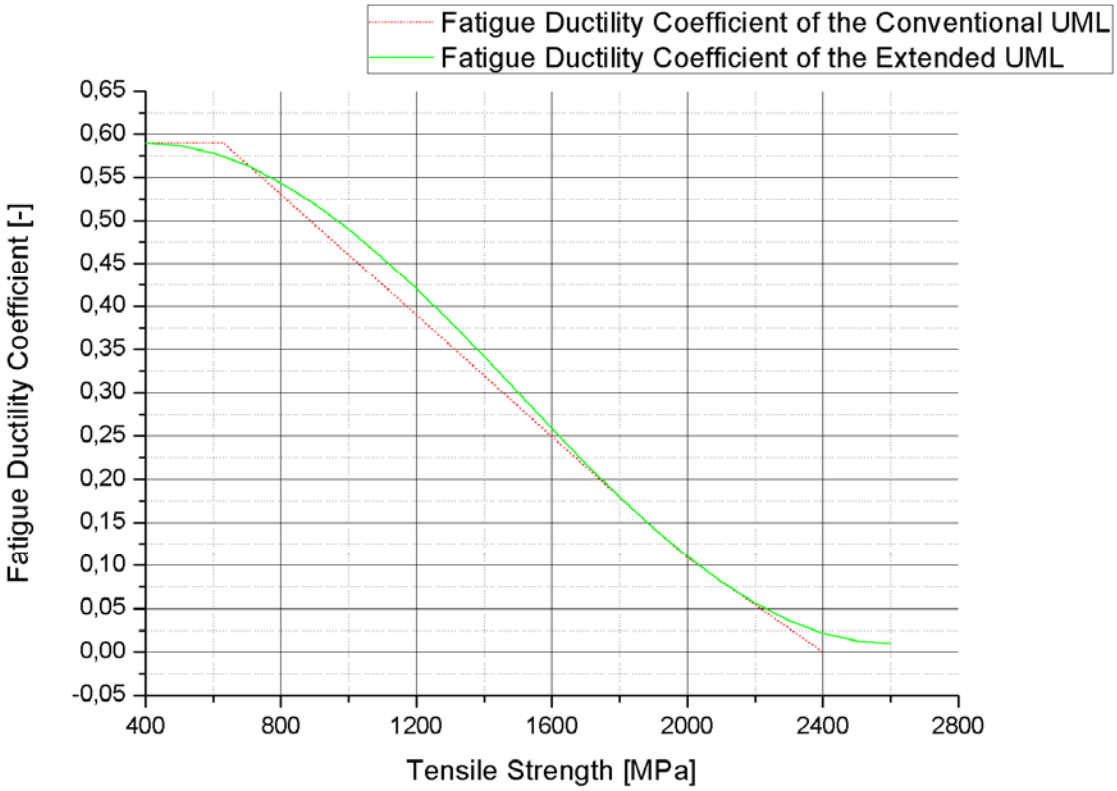

Figure 30. Used Fatigue Ductility Coefficients with Respect to Tensile Strengths

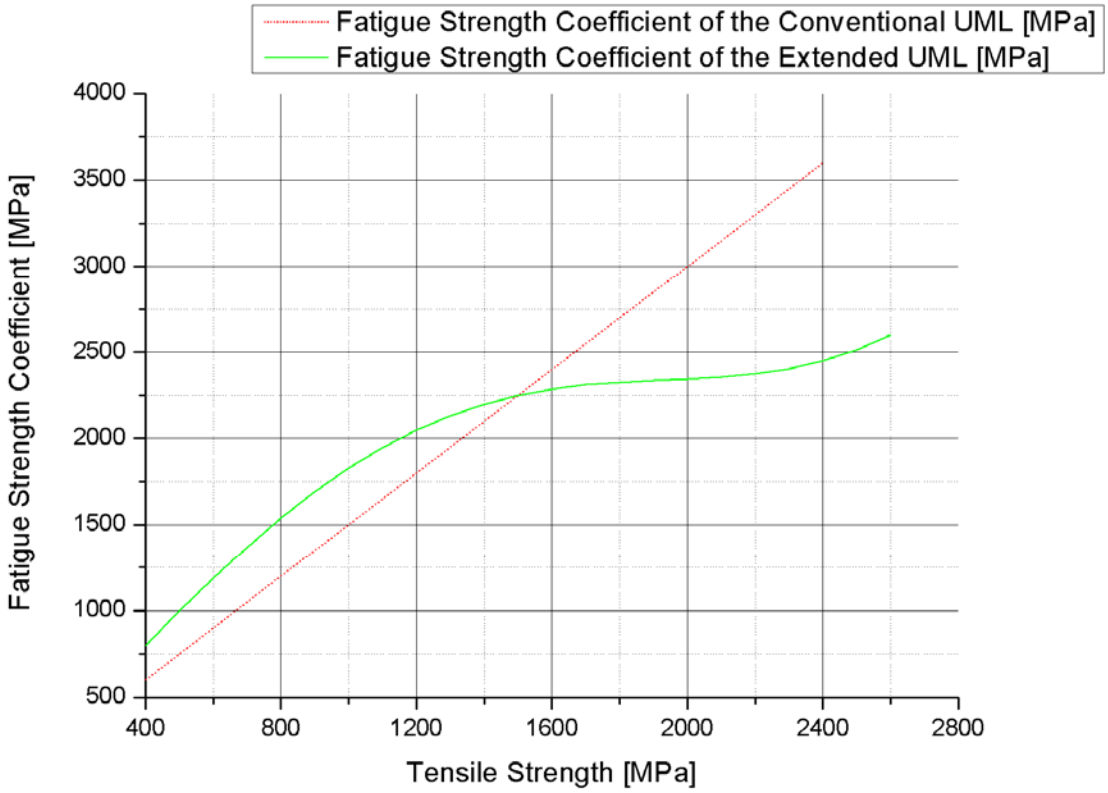

Figure 31. Used Fatigue Strength Coefficients with Respect to Tensile Strengths

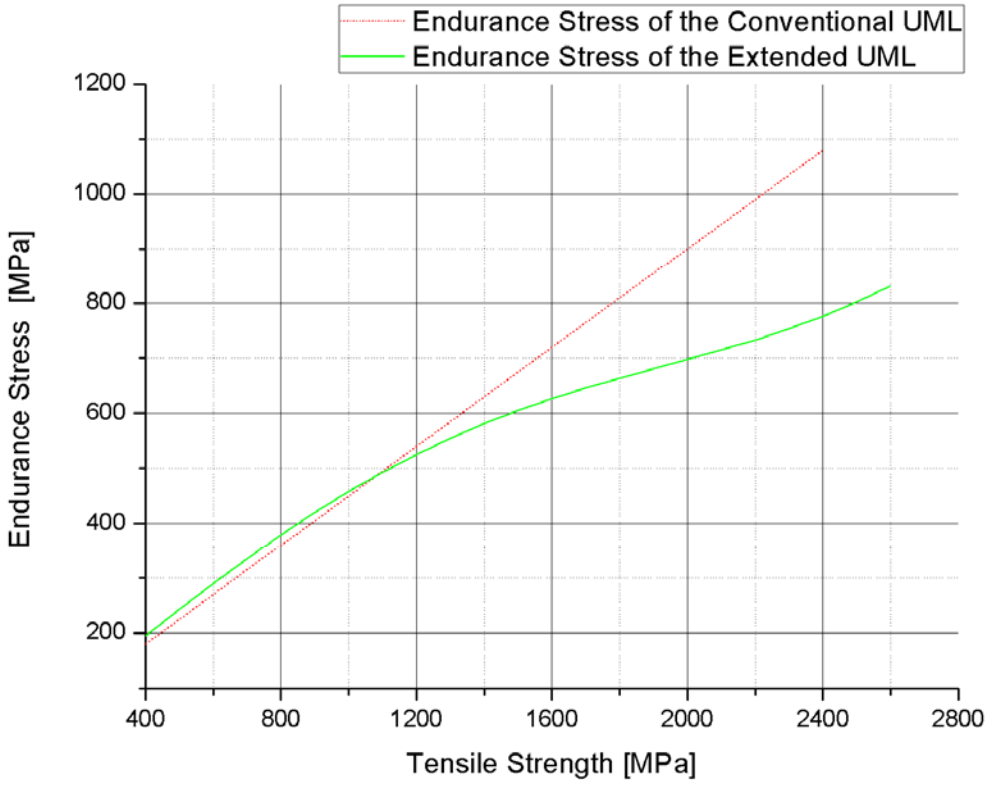

Figure 32. Used Endurance Stress Values with Respect to Tensile Strengths

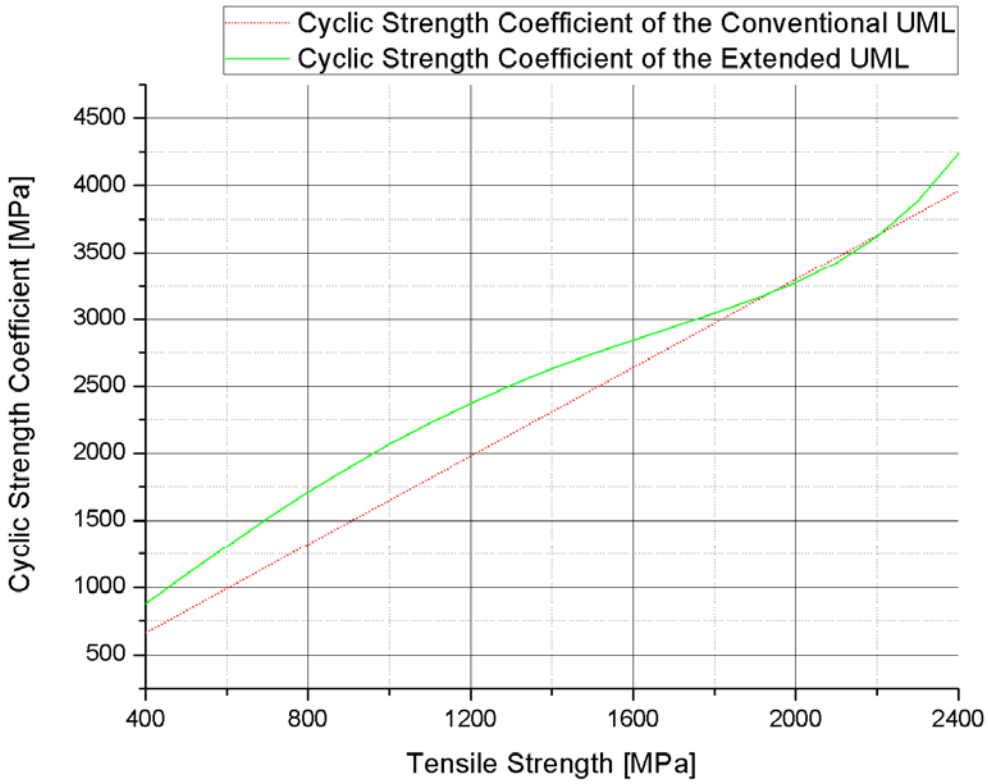

Figure 33. Used Cyclic Strength Coefficient Values with Respect to Tensile Strengths

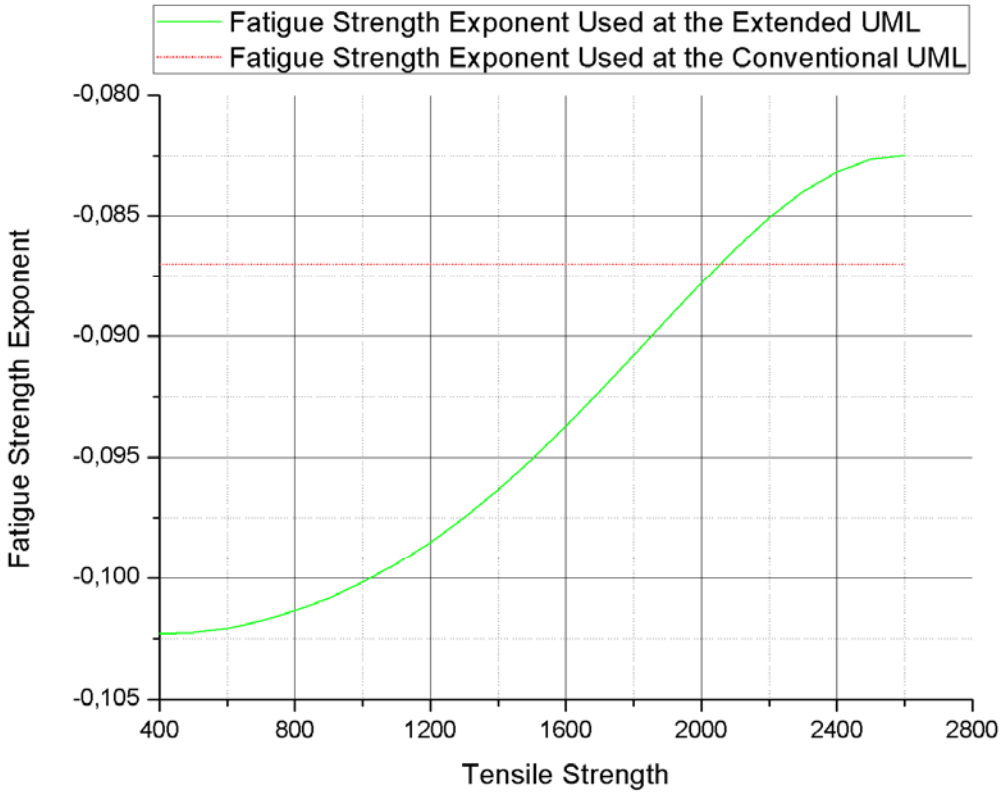

Figure 34. Fatigue Strength Exponent – Tensile Strength Relationships for the Conventional UML and the Extended UML

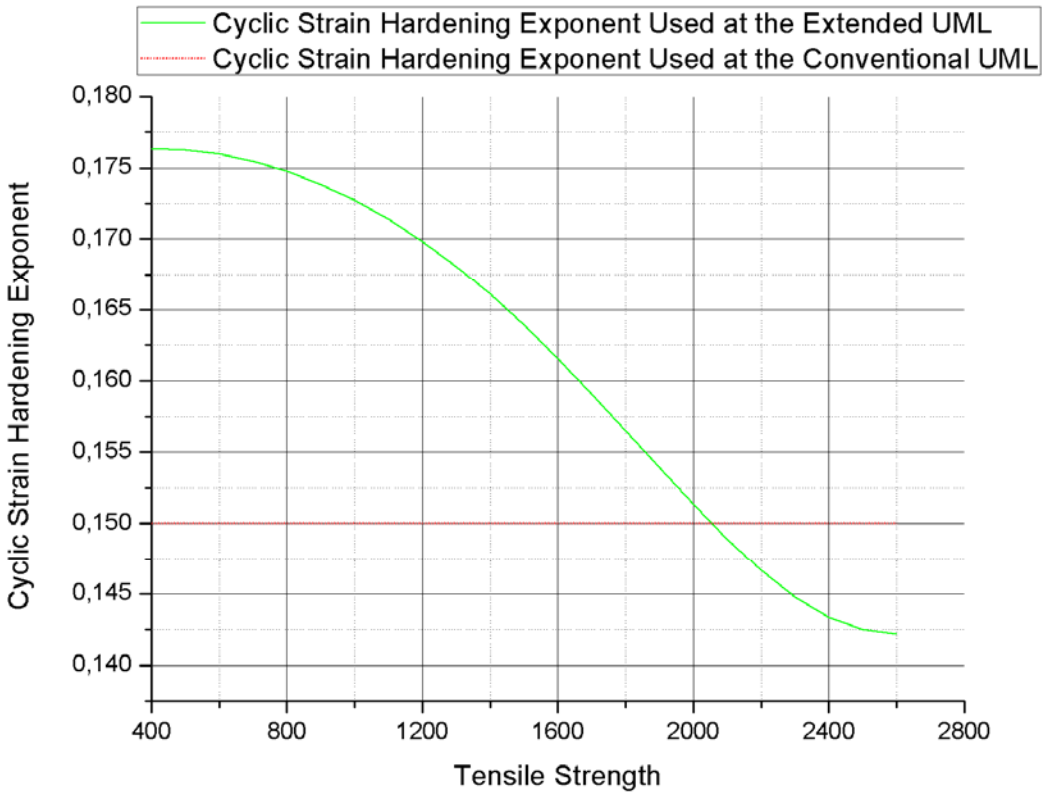

Figure 35. Cyclic Strain Hardening Exponent – Tensile Strength Relationships for the Conventional UML and the Extended UML

The formulas used in order to obtain the graphs above are summarized in the following table:

	Conventional UML	Extended UML
$\mathbf{R_m}$	400 ~ 2400	400 ~ 2400
E	210000	210000
K'	$1.61 \cdot R_m$	$\sigma_f' / (\varepsilon_f')^{n'}$
n'	0.15	b / c
$\boldsymbol{\sigma_f'}$	$1.5 \cdot R_m$	$R_m \cdot (1 + \psi)$
$\boldsymbol{\varepsilon_f'}$	$0.59 \cdot \psi$	$0.58 \cdot \psi + 0.01$
b	-0.087	$-\log (\sigma_f' / \sigma_E) / 6$
$\boldsymbol{\sigma_E}$	$0.45 \cdot R_m$	$R_m \cdot (0.32 + \psi / 6)$
c	-0.58	-0.58
$\mathbf{N_E}$	500000	500000
$\boldsymbol{\psi}$	$\psi = 1.0$ for $(R_m / E) \leq 3 \cdot 10^{-3}$ $\psi = 1.375 - 125 \cdot (R_m / E)$ for $(R_m / E) > 3 \cdot 10^{-3}$ and $\psi \geq 0$	$0.5 \cdot (\cos (\Pi \cdot (Rm - 400) / 2200) + 1)$

Table 4. Used Formulas in UML Calculations

The values obtained can be compared for the tensile strength steps via the following table:

R_m	ψ for Conventional UML	ψ for Extended UML
400	1	1.00000
800	0.89881	0.92063
1200	0.66071	0.70771
1600	0.42262	0.42884
2000	0.18452	0.17257
2400	0	0.02025

Table 5. Calculated Psi Values for the Conventional UML and the Extended UML with respect to Tensile Strengths

R_m	ε_f' of Conventional UML	ε_f' of Extended UML
400	0.590	0.590
800	0.530	0.544
1200	0.389	0.420
1600	0.249	0.259
2000	0.108	0.110
2400	0	0.022

Table 6. Calculated Fatigue Ductility Coefficient Values for the Conventional UML and the Extended UML with respect to Tensile Strengths

R_m	σ_f' of Conventional UML	σ_f' of Extended UML
400	600	800
800	1200	1537
1200	1800	2049
1600	2400	2286
2000	3000	2345
2400	3600	2449

Table 7. Calculated Fatigue Strength Coefficient Values for the Conventional UML and the Extended UML with respect to Tensile Strengths

R_m	σ_E of Conventional UML	σ_E of Extended UML
400	180	195
800	360	379
1200	540	526
1600	720	626
2000	900	698
2400	1080	776

Table 8. Calculated Endurance Stress Values for the Conventional UML and the Extended UML with respect to Tensile Strengths

R_m	K' of Conventional UML	K' of Extended UML
400	660	878
800	1320	1709
1200	1980	2374
1600	2640	2844
2000	3300	3275
2400	3960	4240

Table 9. Calculated Cyclic Strength Coefficient Values for the Conventional UML and the Extended UML with respect to Tensile Strengths

6.2. Comparison of the Stress Amplitude – Strain Amplitude Relationships of the Conventional UML and the Extended UML

The following graphs depict the results of the two calculation procedures in a comparing manner:

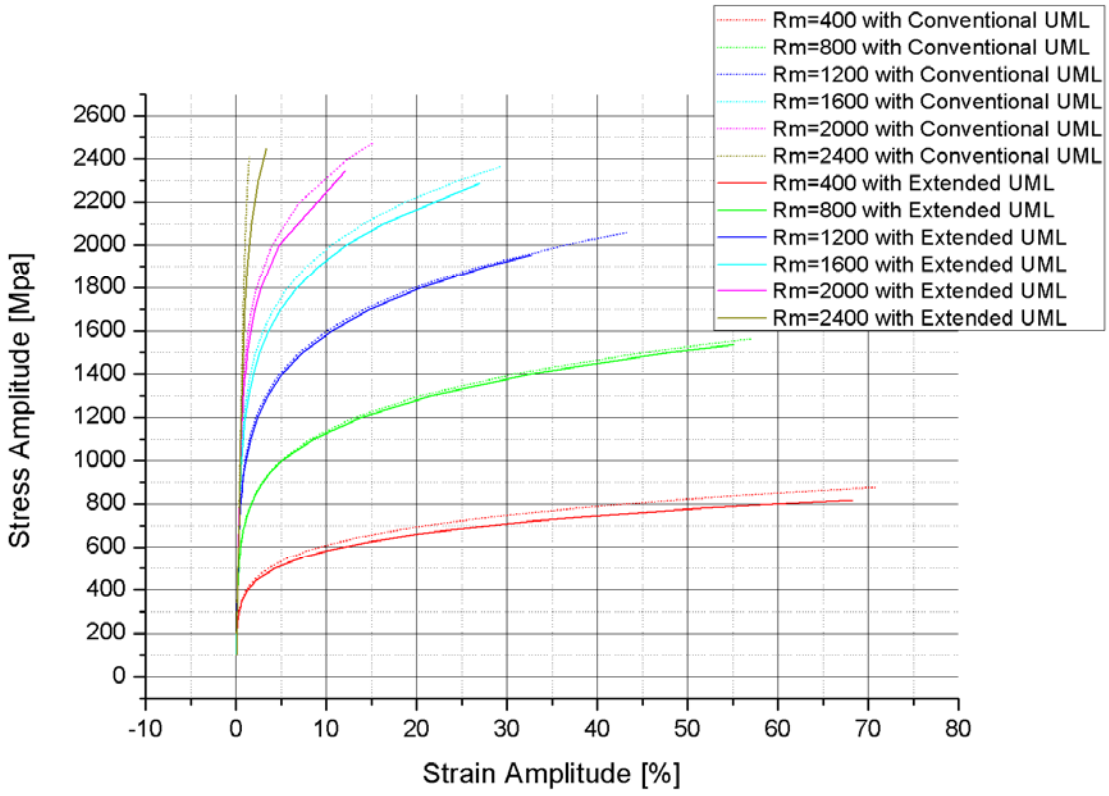

Figure 36. Stress Amplitude – Strain Amplitude Relationships of the Conventional UML and the Extended UML in Linear Scales

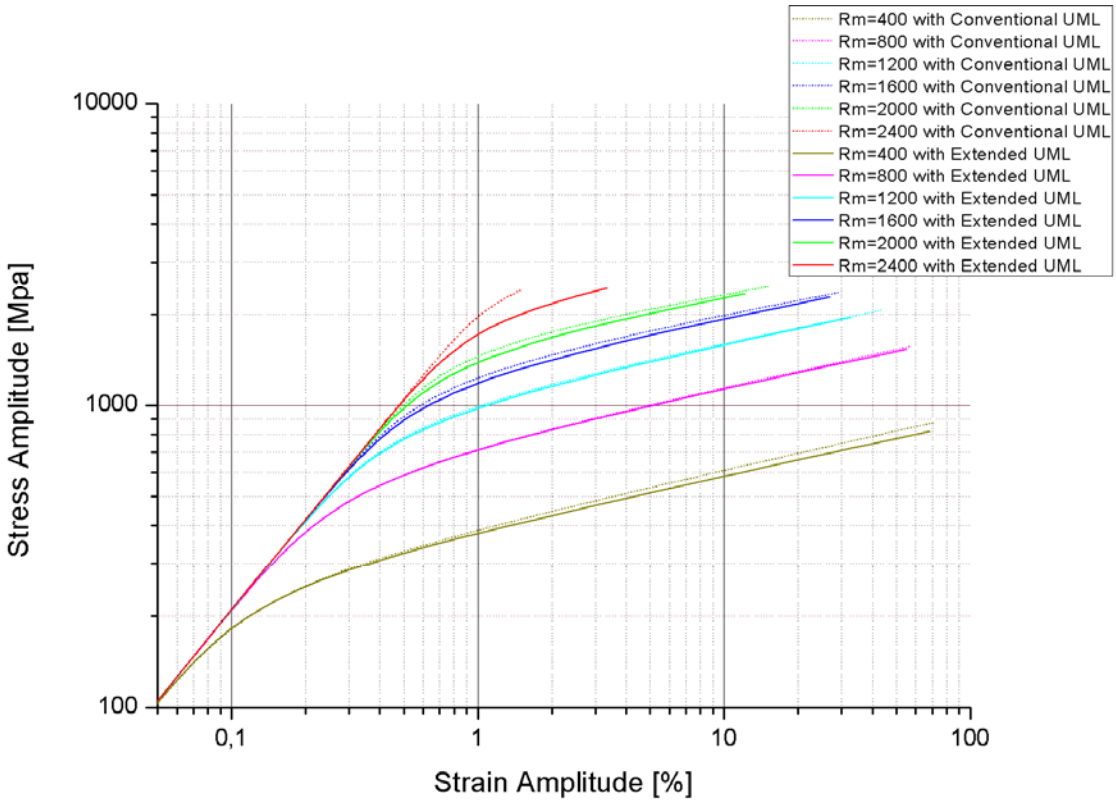

Figure 37. Stress Amplitude – Strain Amplitude Relationships of the Conventional UML and the Extended UML in Logarithmic Scales

6.3. Comparison of the Strain Amplitude – Load Cycle Relationships of the Conventional UML and the Extended UML

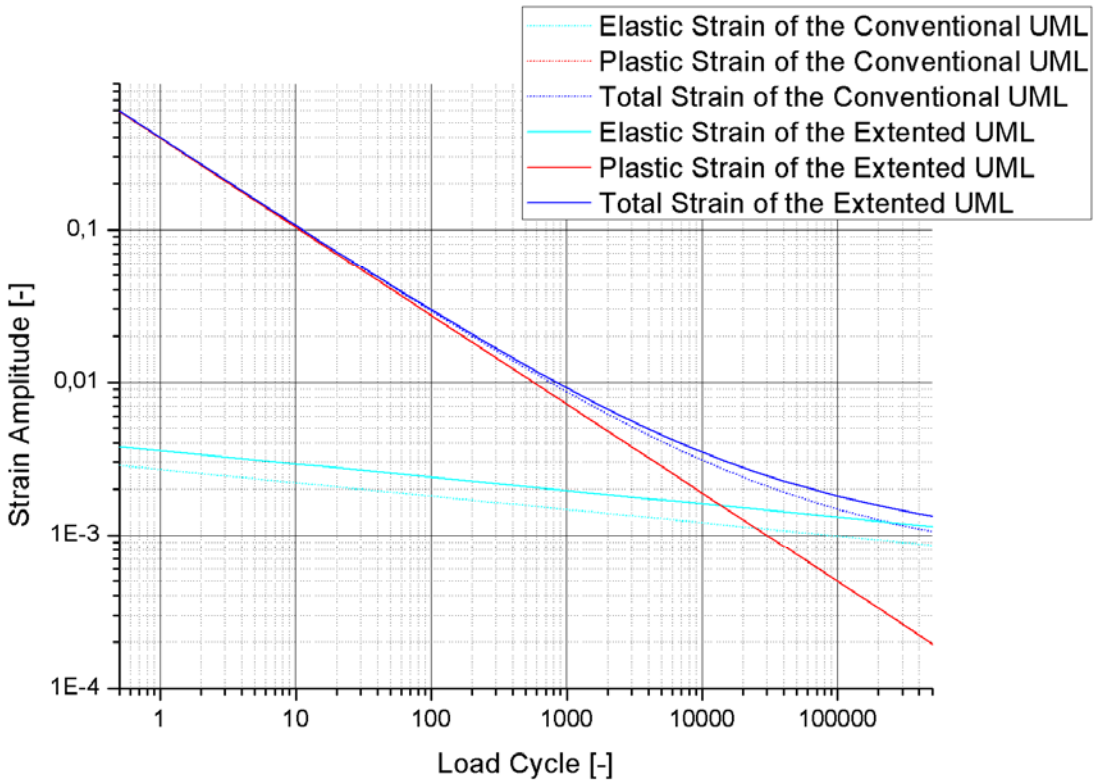

Figure 38. Comparison between the Strain Amplitude – Load Cycle Data of the Steel with the Tensile Strength of 400 MPa in Accordance with the Conventional UML and the Strain Amplitude – Load Cycle Data of the Steel with the Tensile Strength of 400 MPa in Accordance with the Extended UML

For R_m = 400, the elastic strain amplitude calculated via the conventional UML is smaller than the elastic strain amplitude calculated via the extended UML. In this case, the plastic strains are exactly the same for both procedures for the reason being the used ψ values are the same for both procedures (see Table 2 and Table 3). Hence, the difference between the total strain amplitudes becomes equal to the difference between the elastic strain amplitudes.

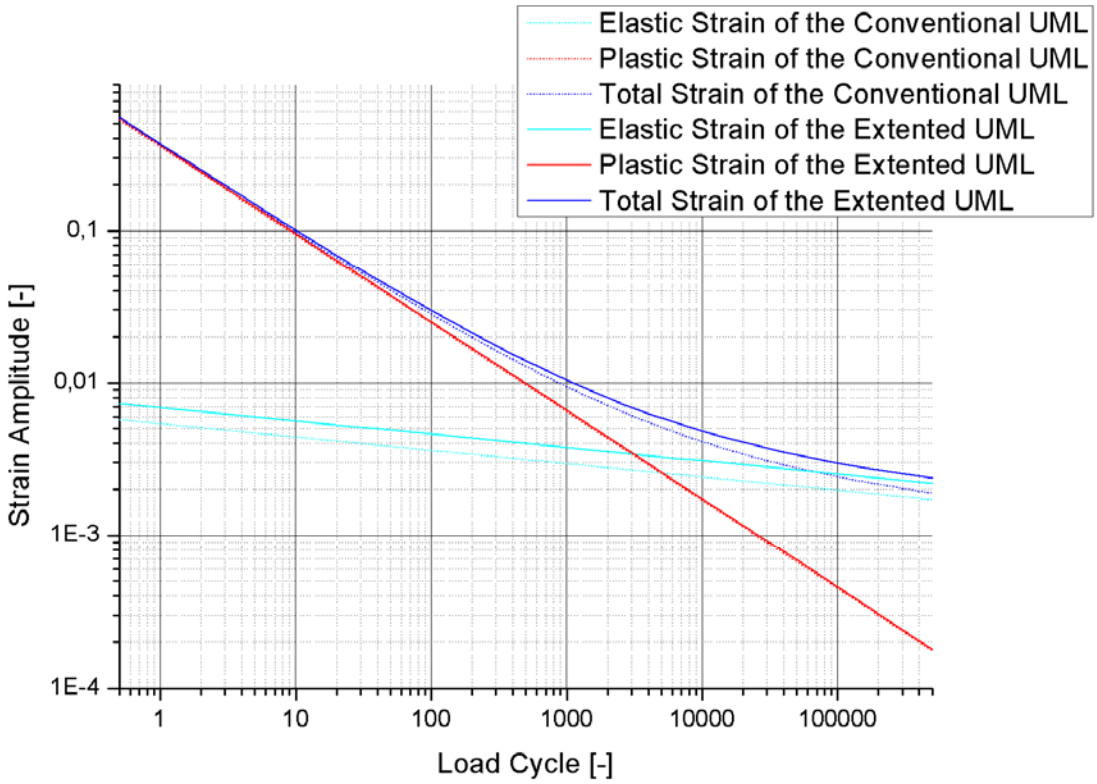

Figure 39. Comparison between the Strain Amplitude – Load Cycle Data of the Steel with the Tensile Strength of 800 MPa in Accordance with the Conventional UML and the Strain Amplitude – Load Cycle Data of the Steel with the Tensile Strength of 800 MPa in Accordance with the Extended UML

For $R_m = 800$, there are slight differences between the results of the conventional UML and the extended UML. The results obtained from the extended UML are slightly greater than the ones obtained from the conventional UML.

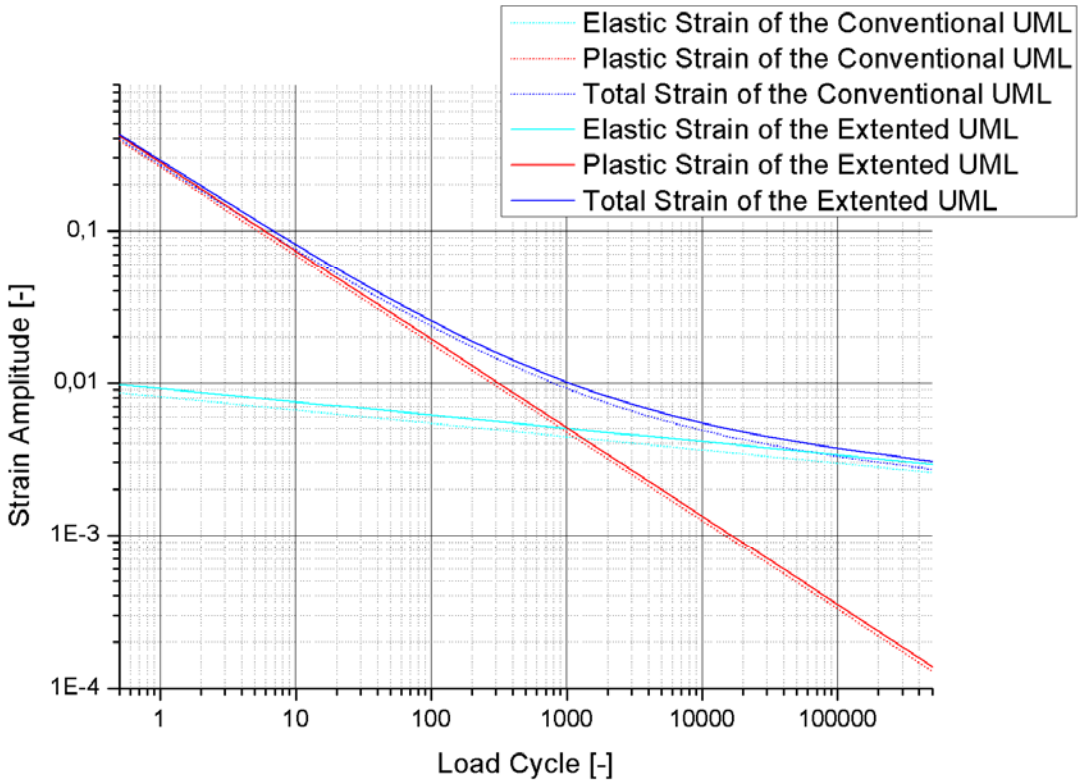

Figure 40. Comparison between the Strain Amplitude – Load Cycle Data of the Steel with the Tensile Strength of 1200 MPa in Accordance with the Conventional UML and the Strain Amplitude – Load Cycle Data of the Steel with the Tensile Strength of 1200 MPa in Accordance with the Extended UML

For $R_m = 1200$, as for $R_m = 800$, slight differences are observed between the results of the conventional UML and the extended UML. The difference between elastic strain amplitudes of the two procedures is apparently bigger than the difference between the plastic strain amplitudes. The extended UML results are slightly greater than the conventional UML results.

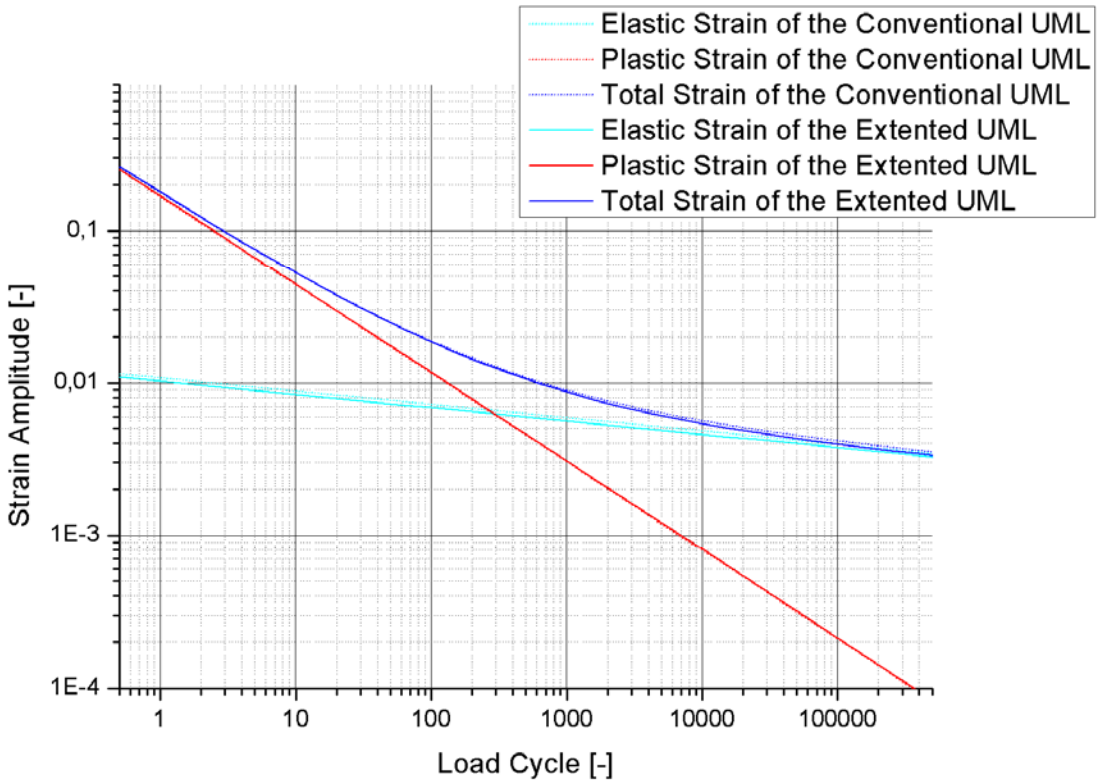

Figure 41. Comparison between the Strain Amplitude – Load Cycle Data of the Steel with the Tensile Strength of 1600 MPa in Accordance with the Conventional UML and the Strain Amplitude – Load Cycle Data of the Steel with the Tensile Strength of 1600 MPa in Accordance with the Extended UML

For $R_m = 1600$, as well, the differences are slight. On the other hand, the extended UML results of elastic strain amplitude, plastic strain amplitude and total strain amplitude are smaller than the conventional UML results for every load cycle, unlike the results for $R_m = 400$, $R_m = 800$ and $R_m = 1200$.

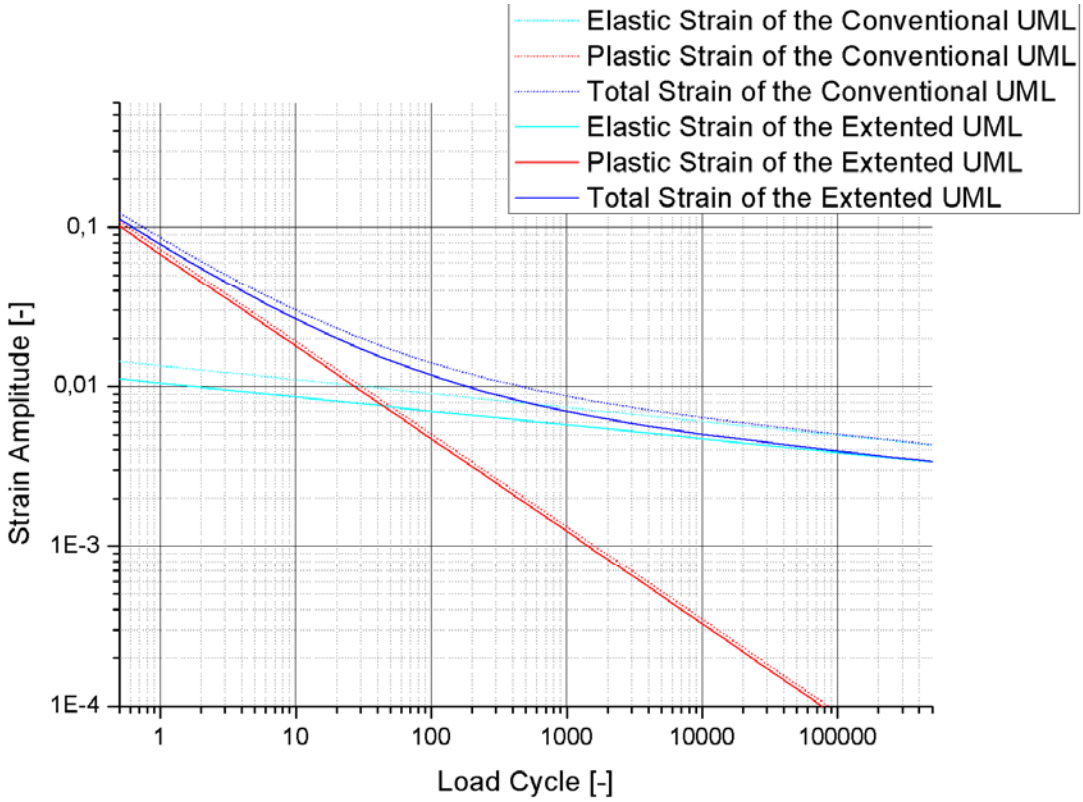

Figure 42. Comparison between the Strain Amplitude – Load Cycle Data of the Steel with the Tensile Strength of 2000 MPa in Accordance with the Conventional UML and the Strain Amplitude – Load Cycle Data of the Steel with the Tensile Strength of 2000 MPa in Accordance with the Extended UML

For R_m = 2000, the results are akin to that of R_m = 1600. The results of conventional UML elastic strain amplitude, plastic strain amplitude and total strain amplitude are greater than the extended UML results for every load cycle. For this level of tensile strength, the differences between the results of the two procedures are even bigger than the differences between the results of the two procedures for the lower adjacent tensile strength step, namely R_m = 1600.

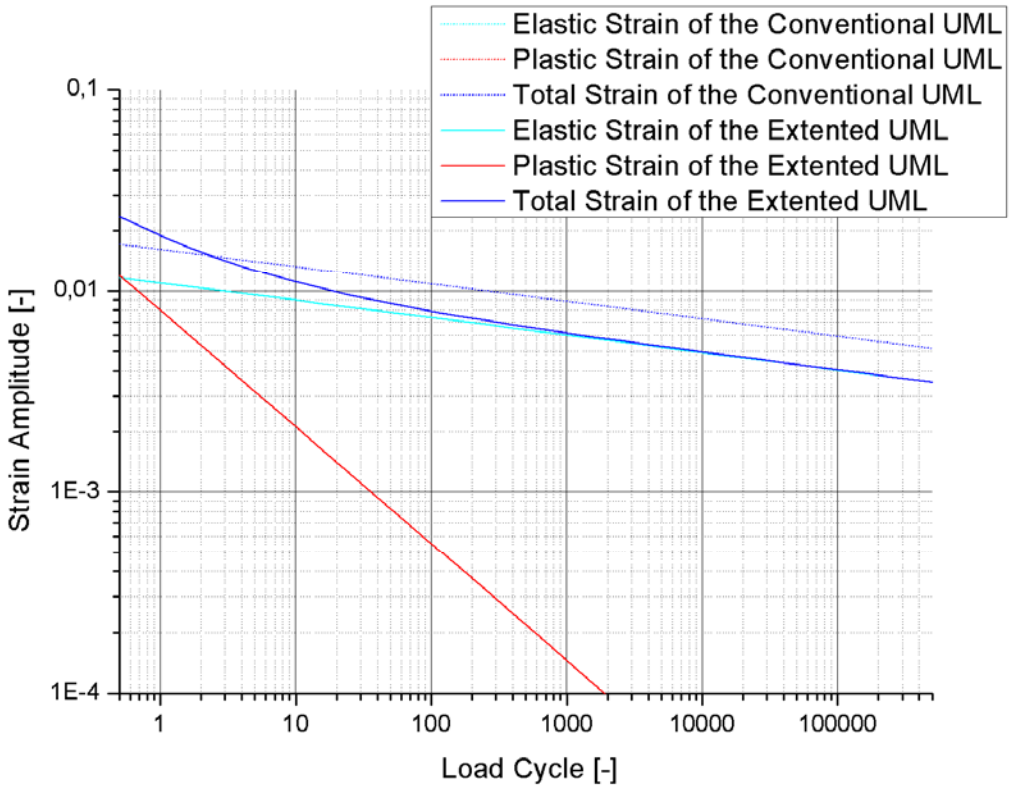

Figure 43. Comparison between the Strain Amplitude – Load Cycle Data of the Steel with the Tensile Strength of 2400 MPa in Accordance with the Conventional UML and the Strain Amplitude – Load Cycle Data of the Steel with the Tensile Strength of 2400 MPa in Accordance with the Extended UML

The results for $R_m = 800$, $R_m = 1200$, $R_m = 1600$, $R_m = 2000$ show a general tendency to have greater values of extended UML and bigger differences as the tensile strength gets higher. This tendency disappears abruptly for the tensile strength step of $R_m = 2400$. The reason for this change is that the plastic strain amplitude for this step becomes zero. That is, the material is expected to show negligible plastic deformation under the assumptions of the conventional UML. However, the extended UML yields the estimate that a considerable greatness of plastic strain amplitude is to be expected for the reason that the conventional UML assumes that:

$$\varepsilon_{a,pl} = 1.375 - 125 \cdot (R_m / E)$$

for

$$R_m / E > 3 \cdot 10^{-3}$$

and

$$\psi \geq 0$$

Nevertheless, in this case,

$$\psi = - 0.05357$$

Hence, ψ is taken into account as $\psi = 0$, which brings us via conventional UML to a solution of merely elastic strain amplitudes that are equal to the total strain amplitudes. On the other hand, for the extended UML,

$$\psi = 0.5 \cdot (\cos (3.1416 \cdot (R_m - 400) / 2200) + 1)$$

The above formula yields a positive ψ. Consequently, the plastic strain amplitudes are estimated to be considerable for the extended UML.

6.4. Comparison of the Smith, Watson, and Topper Parameter Values of the Calculations with the Conventional UML

In 1970 Smith, Watson and Topper introduced the energy parameter, $P_{SWT,}$ into description of the fatigue characteristics of the materials for low- and high-cycle regime. [5]

$$P_{swt} = \sqrt{\sigma_f'^2 \cdot (2N)^{2b} + \varepsilon_f' \cdot \sigma_f' \cdot E \cdot (2N)^{b+c}}$$

Then, the energy fatigue models have been progressively developed. These models are particularly good for description of fatigue properties of the materials not only under uni axial loading but also under multiaxial loading. [6, 7]

The Smith, Watson and Topper Parameter values calculated by using the conventional UML are depicted in the following figure:

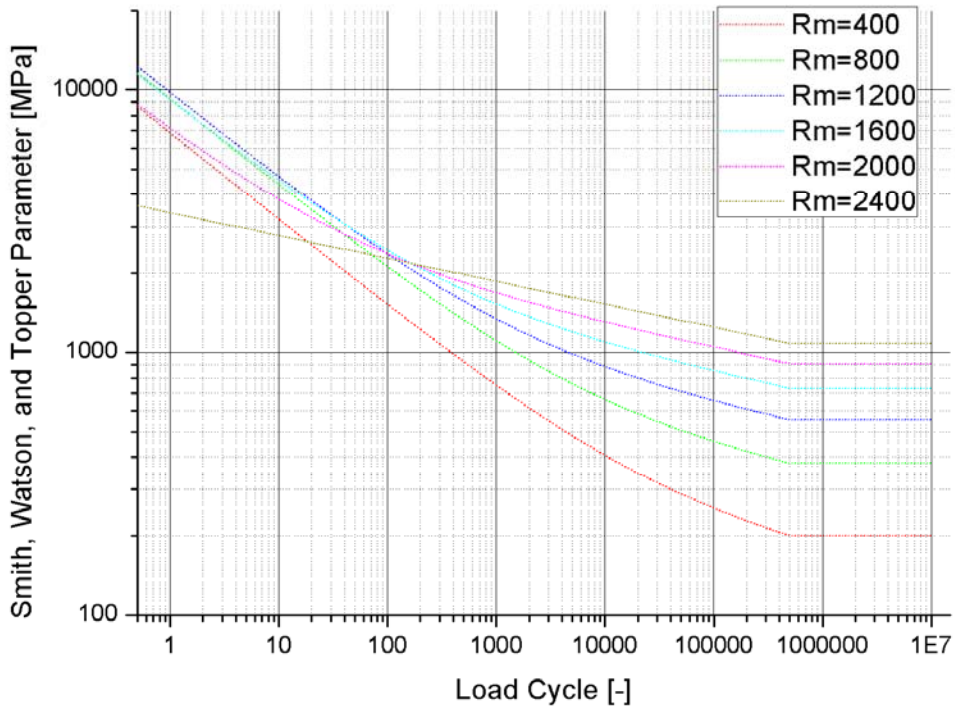

Figure 44. Smith, Watson, and Topper Parameter Values of the Calculations with the Conventional UML with Regard to Load Cycles in Logarithmic Scales

The same parameter is calculated for the Extended UML values, as well. The results are as follows:

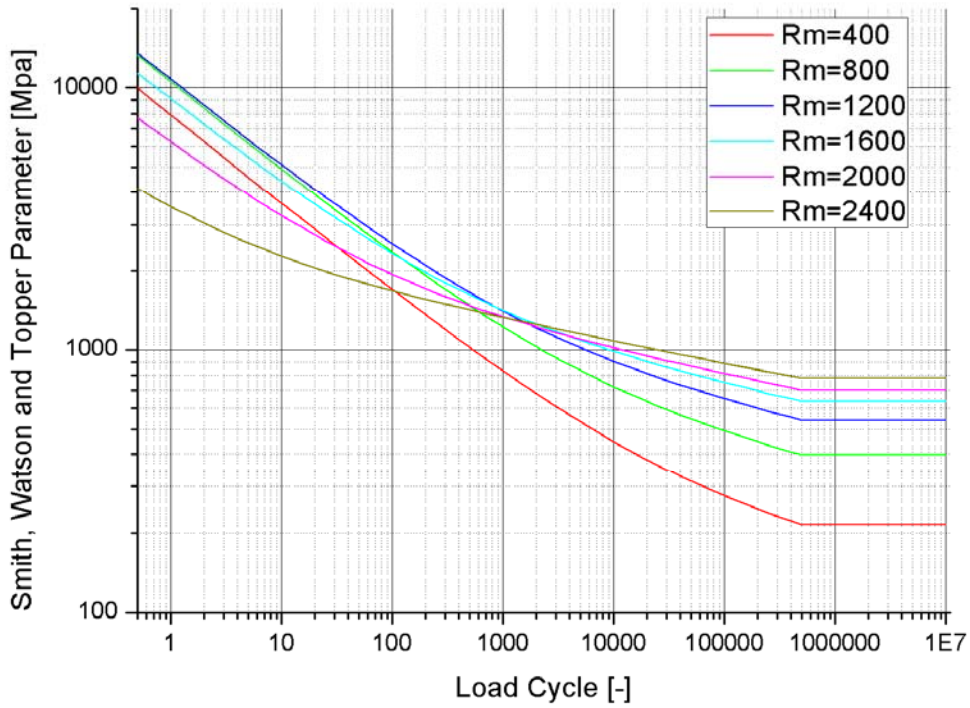

Figure 45. Smith, Watson, and Topper Parameter Values of the Calculations with the Extended UML with Regard to Load Cycles in Logarithmic Scales

Smith, Watson, and Topper Parameter is assumed to be constant after the endurance threshold. These threshold values are computed for each tensile strength step as shown in the below figure:

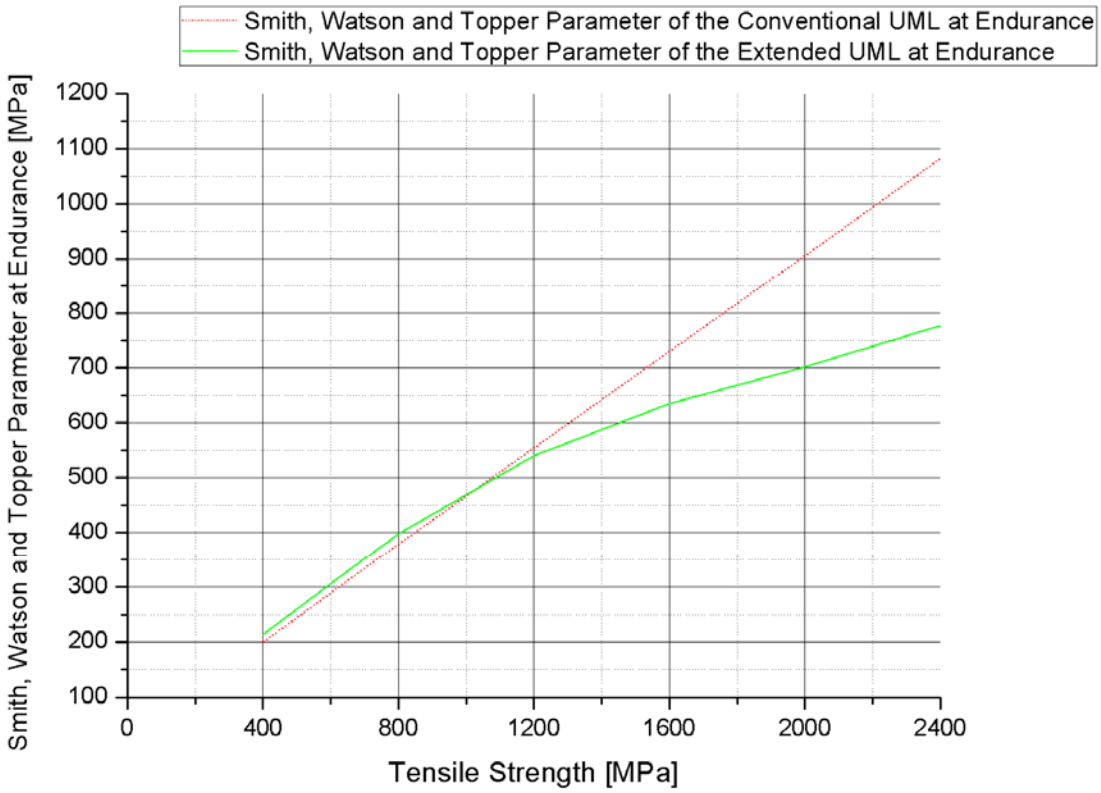

Figure 46. Smith, Watson, and Topper Parameter Values of the Calculations with the Conventional UML and the Extended UML with regard to Tensile Strengths

The following figure shows the Smith, Watson, and Topper Parameter Values of the Conventional UML and the Extended UML together so that a comparison can be made between the values of each approach.

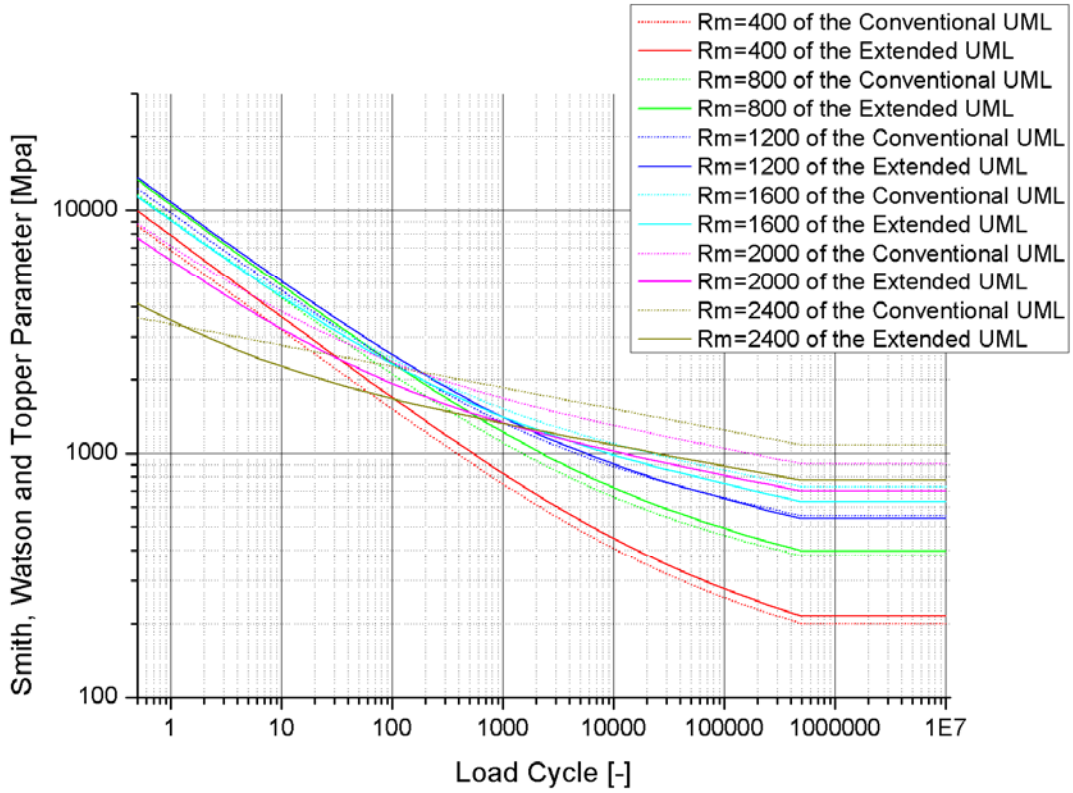

Figure 47. Smith, Watson, and Topper Parameter Values of the Calculations with the Conventional UML and the Extended UML with Regard to Load Cycles in Logarithmic Scales

Finally, the linearization of the Smith, Watson, and Topper Parameter curves has been carried out. The result is as follows:

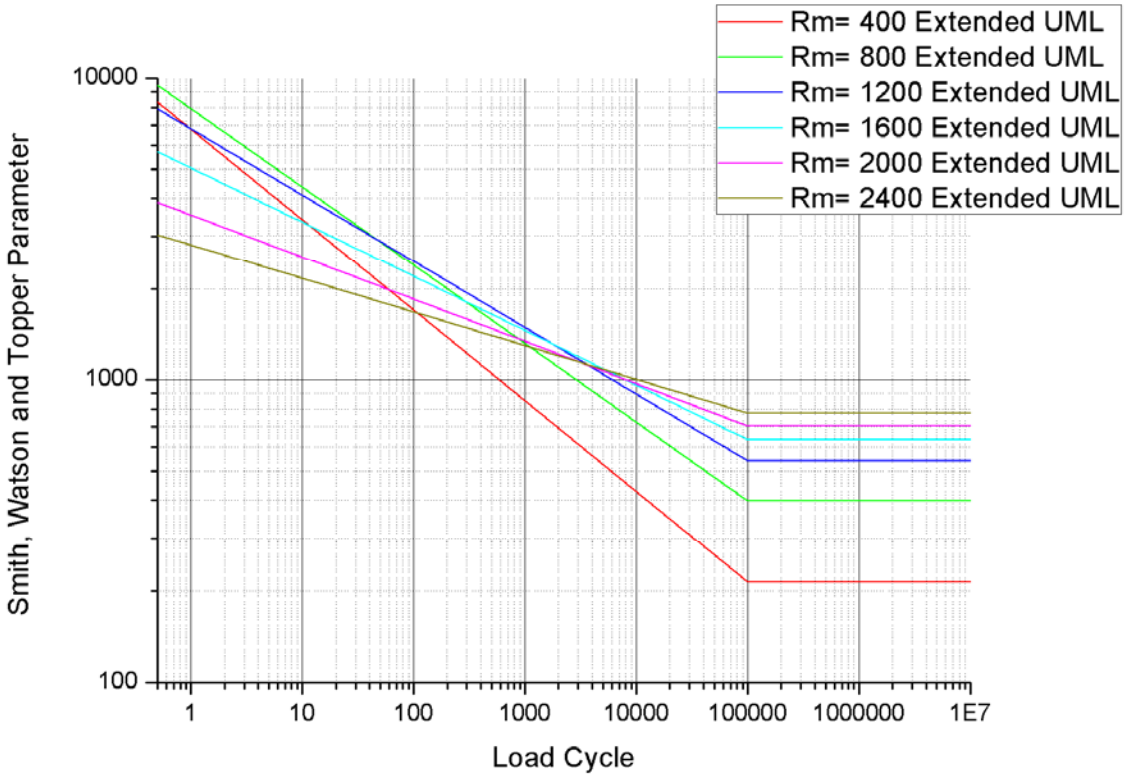

Figure 48. Linearized Smith, Watson and Topper Parameters for Extended UML

7. Life Predictions

The local strain-stress concept is the basis of the most popular crack initiation prediction technique. The basic principle of the local stress-strain approach is that, at the critical point, the local fatigue response of the material, that is, the site of crack initiation is similar to the fatigue response of a tiny, smooth specimen exposed to the same cyclic strains and stresses. From the smooth specimen, which characterizes the material, the cyclic stress-strain response of the material can be found out through proper laboratory testing. In order to perform such laboratory tests properly, the local cyclic stress-strain history at the critical point must be determined. This can be done either by analytical or experimental techniques. Hence, suitable stress analysis procedures, finite element modeling or experimental strain measurements are needed. In this study, experimental strain measurement is used. It must be kept in the mind

that the specimen may undergo cyclic hardening (see Figure 8 and Figure 9), cyclic softening (see Figure 6 and Figure 7), and cycle-dependent stress relaxation, as well as sequential loading effects and residual stress effects, as it accumulates fatigue damage supposed to be the same as at the critical point in the structural member being simulated. [4]

The life prediction computations of the extended UML were applied for 100Cr6 steel. The experimental data is taken from Bomas at all [8] for comparison. The following table depicts the results for smooth specimen and notched specimens with 1 mm and 2 mm radii:

R	ρ	K_t	$S_{a,E}$	m	A_{eff}	V_{eff}	χ*	n_σ	f_r	$S_{a,E}(\chi^*)$	f_{st}	$S_{aE,area}$	V	$S_{aE,vol}$	$S_{aE,min}$	$S_{aE,exp}$
-1	∞	1	813	20	556	516	0	1.00	0,937	771,151	0,995	767,069	1,034	851	**767**	**813**
1	1	2,07	541	20	8,6	0,221	2	1,04	0,937	387,438	1,225	456,449	1,523	606	**456**	**541**
-1	0,2	4,17	305	20	2.0	0,007	10	1,06	0,937	196,024	1,318	243,725	1,810	357	**244**	**305**
0,1	∞	1	535	20	556	516	0	1.00	0,937	517,304	0,995	534,704	1,034	571	**535**	**535**
0,1	1	2,07	355	20	8,6	0,221	2	1,04	0,937	249,905	1,225	366,035	1,523	391	**366**	**355**
0,1	0,2	4,17	200	20	2.0	0,007	10	1,06	0,937	124,054	1,318	211,860	1,810	226	**212**	**200**

Table 10. Parameters Used in the Life Prediction Process

Here,

$$S_{a,E}(\chi^*) = \sigma_{aE-1} \cdot n_\sigma \cdot f_r / K_t$$

$$f_{st} = (A_{eff} / A_{standard})^{(-1 / m)}$$

$$S_{aE,area} = \sigma_{aE-1} \cdot f_r \cdot f_{st} / K_t$$

$$V = (V_{eff} / V_{standard})^{(-1 / m)}$$

$$S_{aE,vol} = (S_{a,E}(\chi^*) / n_\sigma) \cdot V / f_r$$

$$S_{aE,min} = \min (S_{aE,area} ; S_{aE,vol})$$

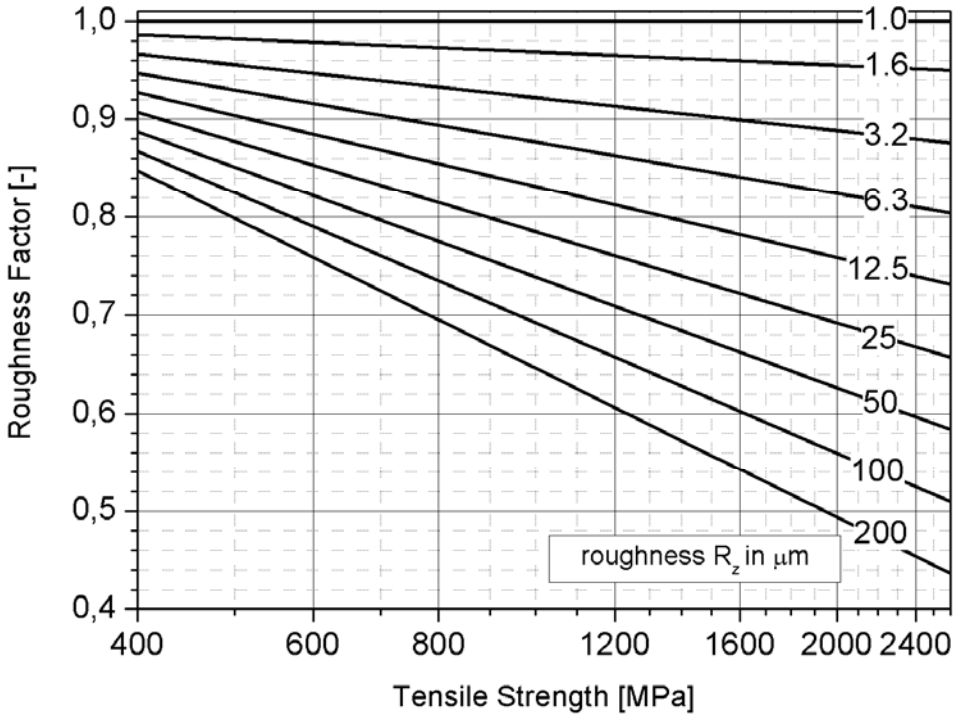

Figure 49. Roughness Factors for Steels with Different Tensile Strengths [9]

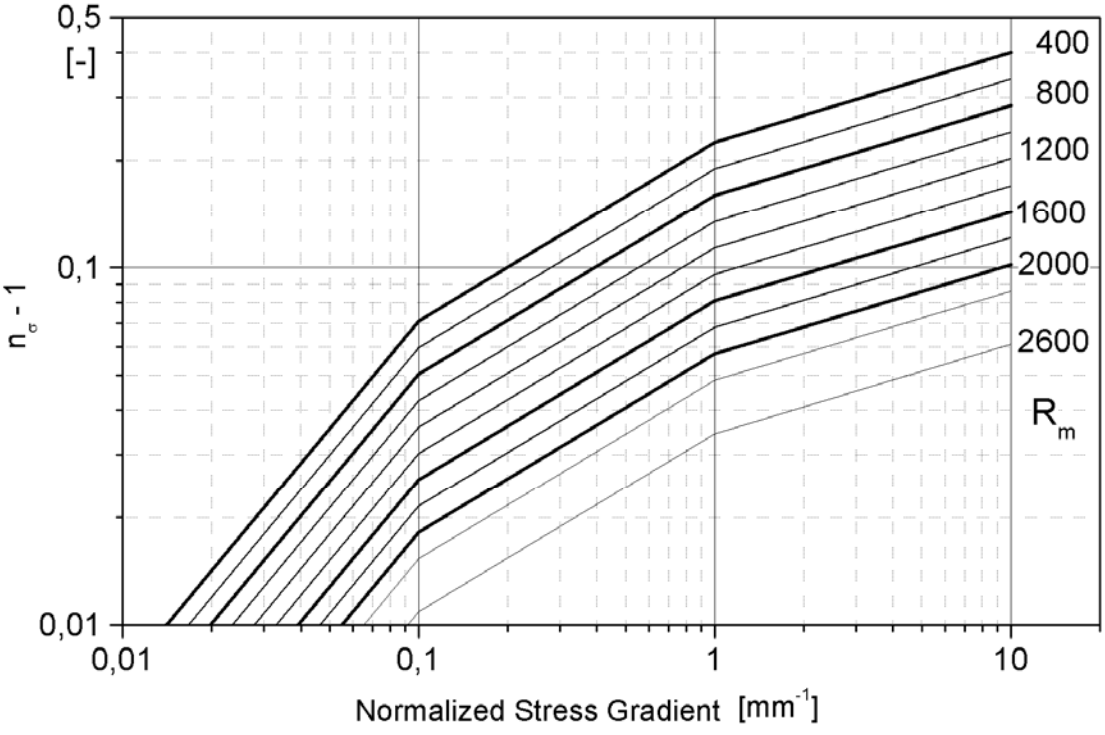

Figure 50. Size Factors for Steels with Different Tensile Strengths [9]

In the calculations, the following values were used as basis:

σ_{aE-1}	823
R_z	1.8
R_m	2600
f_r	0.937

Table 11. Main Values Used at Life Prediction

The figure below shows the ratio of predicted endurance stress and endurance stress obtained from the experiments with regard to the corresponding stress concentration factors:

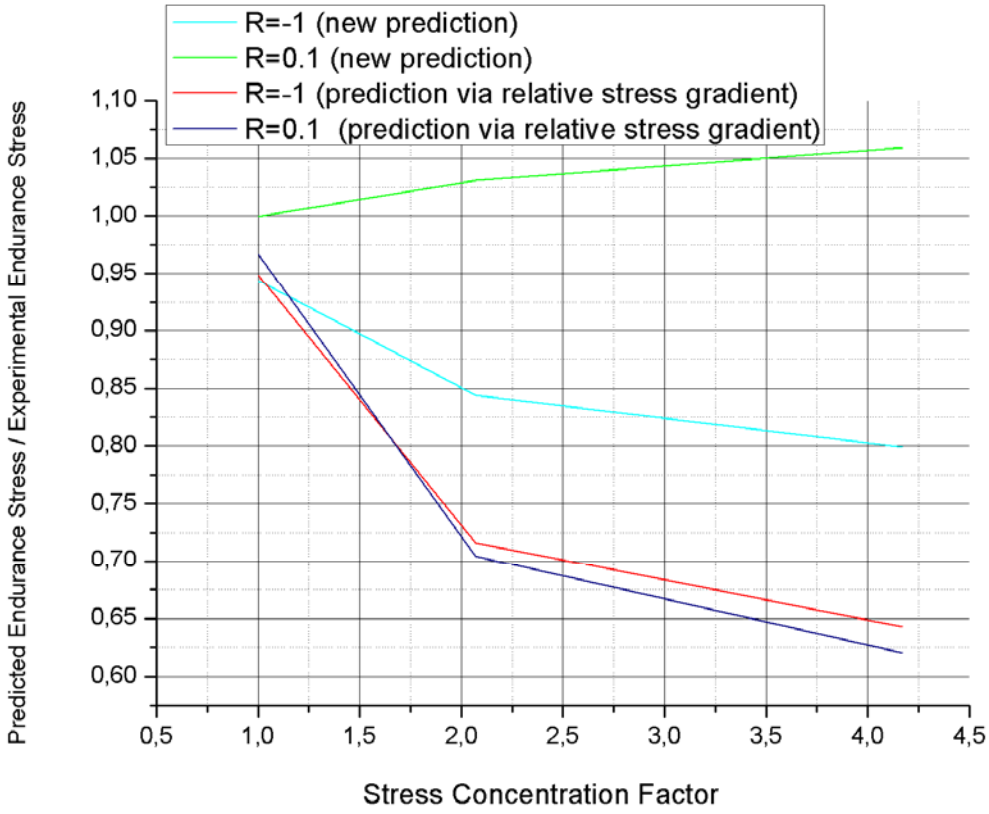

Figure 51. Predicted Endurance Stress / Experimental Endurance Stress Ratios in Accordance with the New Approach and the Classical Approach Using Relative Stress Gradient with Respect to Stress Concentration Factor

It can be observed that the endurance stresses calculated by using the new approach is well better than the prediction made using relative stress gradient. Especially for R=0.1, the

ratio between the predicted endurance stress and the endurance stress obtained from the experiments is between 1 and 1.059. At this case the maximum error is 0.59 %. On the other hand, this value goes down to 0.620 if the prediction is made by using relative stress gradient, which means an error of 38 % at $K_t = 4.17$.

8. Conclusions

The basic motive to carry out the extension of the Uniform Material Law was the need of a more refined approach to predict fatigue behavior of metals. Therefore, the empirical parameters of the conventional UML are defined as functions of material parameters in the proposed extended UML. Cyclic strength coefficient, cyclic strain hardening exponent, fatigue strength coefficient, fatigue ductility coefficient, fatigue strength exponent, endurance stress, and ψ are the major parameters that are defined with rather deterministic functions in the extended UML.

The usage of ψ in the calculation of fatigue strength coefficient has the biggest influence on the difference of the outcomes calculated by the two approaches. In the conventional UML, ψ is used in order to calculate the fatigue ductility coefficient. On the other hand, in the extended UML, ψ is used with the purpose of calculating fatigue strength coefficient, as well. Not only the application area, but also the application method of ψ is different in the two foregoing approaches. In the conventional UML, ψ is a piecewise defined function changing with the threshold of $R_m / E = (R_m / E) = 3 \cdot 10^{-3}$. It is constant for the values under this threshold value. In contrast, in the extended UML, ψ is developed as a cosinusoidal function that it is 1 at $R_m = 400$ MPa and 0 at $R_m = 2600$ MPa. As a result, it could be asserted that the proposed extended UML would be more exact in terms of ψ.

In the conventional UML, fatigue strength coefficient is set as constant. Alternatively, in the extended UML, it is altered by a function of fatigue strength coefficient and endurance stress. In view of the fact that fatigue strength coefficient and endurance stress are related to the tensile strength, the fatigue strength exponent values increase as the tensile strength increases, which leads to an expected decrease in the fatigue strength exponent of the extended UML.

The stress amplitude values calculated by conventional UML are higher than that of extended UML. In spite of higher cyclic strength coefficient values for most of the tensile

strength values of the extended UML, the stress amplitude values calculated by conventional UML are higher than that of extended UML on account of lower cyclic hardening exponent values used in the conventional UML, which is the consequence of fatigue strength exponent function varying with fatigue strength coefficient and endurance stress logarithmically.

The strain amplitude values calculated by the conventional UML are lower than that of extended UML for steels with relatively low tensile strengths. Conversely, for the steels with a tensile strength of 1600 MPa and higher, the strain amplitudes values calculated by the conventional UML become higher than that of extended UML. The relatively big difference becomes smaller until R_m = 1600, and changing its sign at this step. After R_m = 1600, the slight difference gets higher as the steel gets stronger against tensile loading. Thus, one can argue that the extended UML provides higher strain amplitude estimations than that of the conventional for steels with the tensile strength of R_m = 1600 and higher. Then again, for the steels with tensile strengths lower than 1600 MPa, the extended UML presents lower strain amplitude estimations.

The Smith, Watson and Topper parameters at endurance calculated via the results of the extended UML are higher than that of the conventional UML for the steels with tensile strengths lower than 1053 MPa. Conversely, after this tensile strength point, the outcomes of the conventional UML become higher in this context. That is, it can be inferred that the extended UML proposes higher endurance stresses for the steels with tensile strengths lower than 1053 MPa, yet, lower endurance stresses for the steels with tensile strengths higher than 1053 MPa. Vice versa is valid for the conventional UML. Thus, the extended UML is less conservative than the conventional UML for the steels with tensile strengths lower than 1053 MPa, and it is more conservative than the conventional UML for the steels with tensile strengths higher than 1053 MPa. Here, it must be taken into consideration that the differences between the endurance stress proposals of the two approaches are relatively small for the region at which the extended UML proposes higher endurance stresses than that of the conventional UML. On the other hand, the differences between the endurance stress proposals of the two approaches in the region at which the extended UML proposes lower endurance stresses than that of the conventional UML, of which lower tensile strength boundary is 1053 MPa, is are significantly higher. That is to say, the extended UML suggests slightly higher, namely 7 % higher, endurance stress values in the foregoing region, yet, the conventional

UML presents up to 39 % higher values than that of the extended UML within the tensile strength scale between 400 MPa and 2400 MPa.

The life prediction was carried out by using a relatively high Weibull exponent. For high strength metals, this value is used between 15 and 40. However, Weibull exponent is selected as 20, which is a rather high scatter. For R = 0.1, the behavior is considered to be elastic. Furthermore, for high strength materials, such as the ones used in this study, the influence of normalized stress gradient is low. Moreover, support factor for stress gradient is not sufficient for small areas and volumes under high loads. At this point, statistical size effect should be introduced into the computation.

Reference List

1. Understanding Fatigue Analysis, University of Cambridge Department of Engineering Website (http://www.eng.cam.ac.uk/DesignOffice/cad/proewild3/usascii/proe/promec/online/fatigue.htm) [2008]

2. Mechanics of Fatigue, Bolotin, Vladimir V, [1998]

3. Zur Betriebsfestigkeitsbemessung Gekerbter Bauteile auf der Grundlage der örtlichen Beanspruchungen, Bergmann, Joachim W. [1983]

4. Fatigue of Materials, Subra Suresh, Cambridge University Press, [1998]

5. A Stress-Strain Function for the Fatigue of Metals, Smith K. N., Watson P. and Topper T.H., Journal of Materials, Vol. 5, No 4, [1970]

6. Energy Criteria of Multiaxial Fatigue Failure, Macha E., Sonsino C.M., Vol.22, [1999]

7. A Review of Energy-Based Multiaxial Fatigue Failure Criteria, Macha E., The Archive of Mechanical Engineering, Vol.XLVIII, No.1, [2002]

8. Analyse der Ermüdungsrissbildung und Dauerfestigkeit des Stahles 100Cr6 im bainitischem Stand, Bomas H., Linkewitz T., Mayr P., Carl Hanser Verlag, München, [2002]

9. Analytical Strength Assessment of Components in Mechanical Engineering, Forschungskuratorium Maschinenbau (FKM), [2003]

10. Materials Data for Cyclic Loading, Supplement 1, Bäumel, A., Seeger, T., Elsevier Amsterdam, [1990]